SYNAPTIC ORGANISATION OF VISUAL SPACE IN PRIMARY VISUAL CORTEX

Inauguraldissertation

zur

Erlangung der Würde eines Doktors der Philosophie

vorgelegt der

Philosophisch-Naturwissenschaftlichen Fakultät

der Universität Basel

von

Ioana Teodora Gasler

von Rumänien

Basel, 2018

Genehmigt von der Philosophisch-Naturwissenschaftlichen Fakultät auf Antrag von

Prof. Dr. Sonja Hofer, Prof. Dr. Peter Scheiffele

Basel, 14.11.2017

Prof. Dr. Martin Spiess

Dekan der Philosophisch-

Naturwissenschaftlichen Fakultät

Contributions

The experiments included in this thesis, as well as data analysis, were jointly performed by the author and Dr. Maria Florencia Iacaruso.

Acknowledgements

Firstly, my gratitude and admiration for Flor, who had a tremendous contribution to pushing this work forward. It was a great help and relief to share this project with you and I truly believe it would not have gotten so far had it not been for you. Thank you for your friendship, patience and for lending a sympathetic ear when things were not at their best.

Sonja: thank you for being a hands on, dedicated supervisor, for the guidance, for challenging me and for helping me learn. By all this, you have equally supported me in reaching this point, which seemed at times so remote and uncertain.

Maxime, who is very unfortunate to have to compete against Meanhwan for the nicest “desk mate”. Thank you for always taking the time to patiently advise me on my trivial (for you) analysis questions, for the music, the chats, the hikes and all the rest.

Some of the people who lent me their scientific and technical expertise and advise, as well as their friendship: Dylan, Rob, Devon.

Ivana, Peter who took me in (literally) at the very beginning of this journey.

Morgane, Antonin, Francois and Caroline, not enough space and time for everything.

Finally, the friends outside the lab, especially Komal, Philipp, Marc. Thank you for making my life in Basel full and warm and fun and for helping me feel at home.

I am very grateful to you all, and to others who got left out in the rush to submit on time, for so much more than I can compress here. Through all the ups and downs of the last four years, you have made this a wonderful experience and my best decision so far.

To be continued..

Contents

1. General introduction

1.1 THE RETINA

At the first stage of visual processing, photons are captured by the eye and transduced into electrical signals that propagate further across the retinal layers. The main cell types involved in retinal processing are sequentially photoreceptors, bipolar cells and retinal ganglion cells, the latter providing the retinal output

Photon detection is mediated by photoreceptors in the retina containing chromophores. These photo pigments can vary in the wavelengths of light they absorb according to photoreceptor type, rod or cone, but also between species (Bowmaker et al., 1978; Bowmaker and Dartnall, 1980; Röhlich et al., 1994). Generally, rods contain a pigment which absorbs a wider range of wavelengths and is more sensitive to light (Baylor et al., 1979). Rods are thus responsible for vision under low illumination conditions, whereas the pigments contained by cones have narrower bandwidths and mediate color vision (Ebrey and Koutalos, 2001). Chromophores are coupled to proteins called opsins and upon photon absorption they trigger a conformational change. An intracellular cascade is activated, resulting in hyperpolarization of the photoreceptor and decreased synaptic release of glutamate (Yarfitz and Hurley, 1994).

Bipolar cells, the postsynaptic partner of photoreceptors, are a diverse class encoding various stimulus features (Boycott and Wässle, 1991; Euler et al., 2014). Based on their response to glutamate release, they can be categorized as either on or off cells (Werblin and Dowling, 1969). ON bipolar cells are hyperpolarized by glutamate, such that stimulation of photoreceptors, their subsequent hyperpolarization and reduced glutamate release will depolarize these cells, while OFF bipolar cells have the opposite response (Boycott and Wässle, 1991).

The region of visual space in which changes in light intensity lead to activation of a cell is called a receptive field (Hartline, 1938). This is a common feature of most visually responsive neurons regardless of their location in the visual pathway. The receptive fields of bipolar cells have concentric shapes with a center-surround configuration (Kuffler, 1953). This layout is characterized by two separate regions in which illumination has antagonistic effects. The circular region at the center of the receptive field is anatomically defined by the location of the

photoreceptor input (Behrens et al., 2016). Illumination of these photoreceptors generates the center response. Nearby photoreceptors in the annular region surrounding the center do not share a connection with the bipolar cell, but influence its activity indirectly. When the surround photoreceptors are stimulated, they modulate the activity of the center photoreceptors in the opposite direction, generating the surround response of the bipolar cell as illustrated in Figure 1.

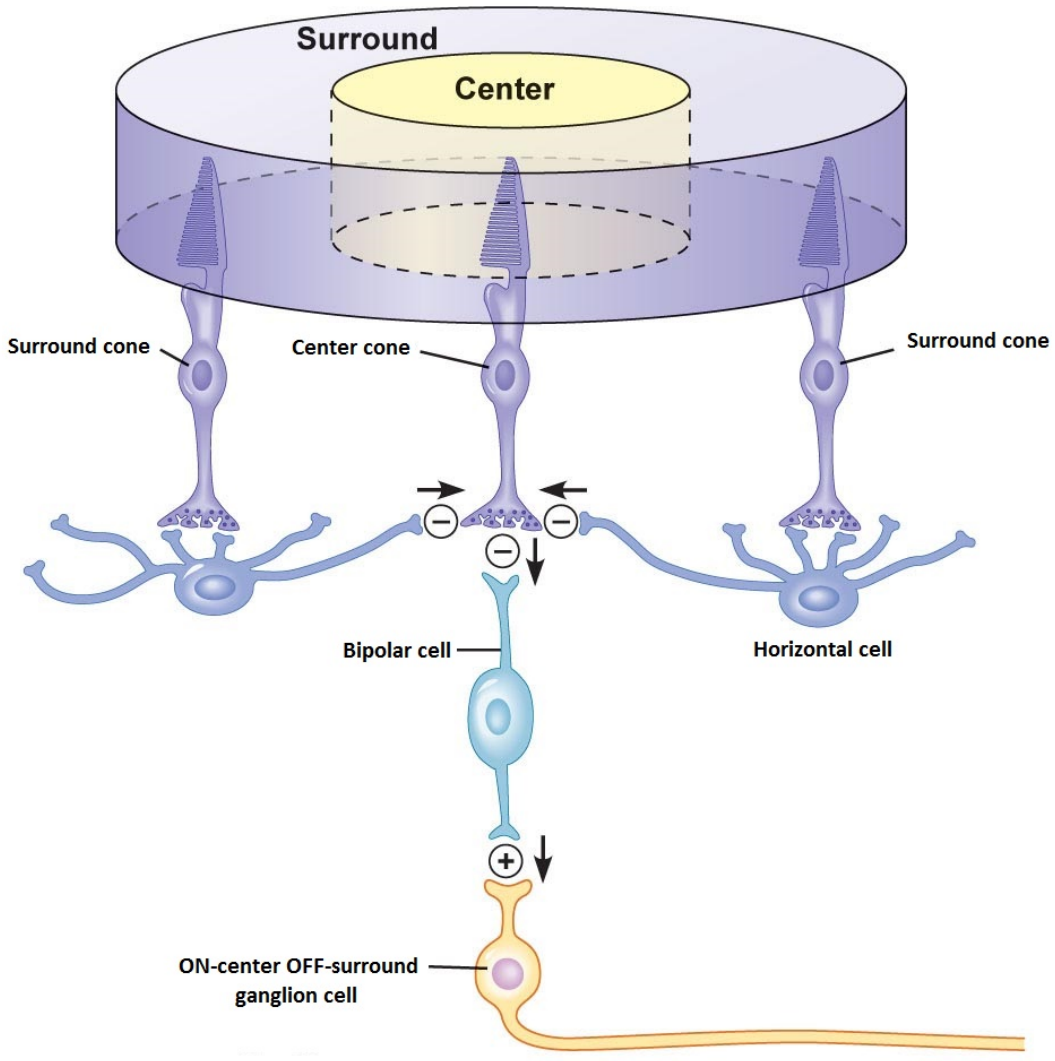

Adapted from N. Carson *Foundations of behavioural neuroscience*

Figure 1 | The retinal center-surround receptive field

Cell types and interactions underlying the structure of an ON-center RF. An incremental light increase at a precise retinal location activates the photoreceptors in that region, which relay this signal to the postsynaptic bipolar cell. The presence of a light stimulus in the surround region will activate a different set of photoreceptors,

which act through horizontal cells to modulate the activity of the center photoreceptor in the opposite direction. As a result, for an ON-center cell, illumination of the center increases activity of the bipolar cell, while illumination of the surround decreases it. The same response pattern is inherited by the postsynaptic RGC.

Different subsets of bipolar cell types provide input to approximately 33 types of retinal ganglion cells (RGCs) (Baden et al., 2016). RGCs have receptive fields with the same center-surround configuration (Famiglietti and Kolb, 1976) while generating a variety of specific functional properties, such as "suppressed by contrast" responses or direction selectivity (Barlow and Hill, 1963; de Monasterio, 1978; Rodieck, 1967; Sun et al., 2006; Tien et al., 2015; Vaney and Taylor, 2002; Weng et al., 2005), involved in different aspects of visual processing. The high diversity of RGCs enables the retina to separately process different features of the visual scene in multiple parallel channels (Baden et al., 2016; Boycott and Wässle, 1999; Dhande et al., 2015; Roska and Werblin, 2001) which are further relayed to downstream targets.

The RGC axons form the optic nerve. They partly cross the midline in the optic chiasm and form the optic tract which relays information to downstream areas in the visual pathway. Axons from the temporal half of the retina remain in the ipsilateral hemisphere while those from the nasal half of the retina cross to the contralateral side. In rodents approximately 95% of retinal ganglion cell axons cross in the optic chiasm (E Reese and Cowey, 1987; Petros et al., 2008).

1.2 THE LATERAL GENICULATE NUCLEUS

The retinal input targets more than 40 subcortical areas (Morin and Studholme, 2014). Many of these are involved in non-image forming circuits, which mediate accessory functions such as eye reflexes and circadian rhythm (Seabrook et al., 2017). The main image forming pathway passes through the lateral geniculate nucleus (LGN) of the thalamus and makes its way to the primary visual cortex.

The retina is the main driver of LGN cells (Sherman and Guillery, 1996; Sincich et al., 2007) and the projection pattern of RGCs in the LGN creates a retinotopic map of visual space, a topographic representation of the sensory periphery on the cortical surface, whereby neighboring neurons respond to activation of neighboring peripheral photoreceptors (Crossland and Uchwat, 1979; E Reese and Cowey, 1987; Eysel and Wolfhard, 1983; Niell, 2013).

Originally the LGN was thought to be a simple relay station to the cortex. This view was supported by the similarity between the functional properties of LGN neurons and those of retinal ganglion cells (Rathbun et al., 2010; Usrey et al., 1999). The classical receptive fields initially identified in the LGN by the pioneering work of Hubel and Wiesel (Hubel, 1960; Hubel and Wiesel, 1962) are similar to those of retinal ganglion cells: concentric on and off (center-surround) regions, suggesting that little to no processing occurs at this level.

However, the activity and response properties of LGN cells are modulated by various sources, including projections from brain stem structures and the superior colliculus, as well as inhibitory input from local interneurons and the thalamic reticular nucleus (Ghodrati et al., 2017). Moreover, LGN receives extensive feedback projections from primary visual the cortex, which exceeds the retinal feed-forward input, and whose role is still unclear (Briggs and Usrey, 2008; Sillito et al., 2006; Sillito and Jones, 2002).

Therefore, in recent years, there has been a shift in the interpretation of LGN function, as data increasingly indicates a higher diversity of response properties and state-dependent response modes arising in the LGN (Cruz-Martin et al., 2014; Fisher et al., 2017; Guido et al., 1992; Piscopo et al., 2013; Sherman and Guillery, 1996; Suresh et al., 2016; Zhao et al., 2013a). For instance, a recent study identifies three patterns of convergence of retinal inputs onto single mouse LGN neurons (Rompani et al., 2017). Contrary to what was previously described (Chen and Regehr, 2000; JAUBERT-MIAZZA et al., 2005), a higher diversity of RGC types can provide input to one LGN cell. Moreover, numerous binocular inputs have been identified, adding to accumulating evidence in different species that not all LGN neurons are monocular, as previously thought (Cheong et al., 2013; Grubb and Thompson, 2003; Howarth et al., 2014).

It remains unclear how geniculate cells integrate these diverse inputs and what response properties the different patterns generate. Recent unpublished work suggests that modulatory corticothalamic feedback might act to select subsets of retinal inputs used by the LGN cells receiving a functionally wide array of connections from retinal ganglion cells (Rompani et al., 2017).

In primates and carnivores, the LGN is divided into clearly separated layers while the rodent LGN shows far less defined boundaries. However, some mouse RGC types show a form of layer-specific targeting (Seabrook et al., 2017). Orientation selective (OS) (Piscopo et al., 2013; Scholl et al.,

2013; Zhao et al., 2013a) and direction selective (DS) cells (Cruz-Martin et al., 2014), which receive input from direction selective ganglion cells, are preferentially located in the posterior and dorsolateral LGN shell region while non-direction selective RGCs synapse onto a separate class of neurons in the LGN core (Niell, 2013; Piscopo et al., 2013). The source of their selectivity is considered to be most likely their retinal input as cortical silencing does not alter orientation selective responses in LGN (Zhao et al., 2013a).

Although more common in mice, LGN cells selective for orientation (Cheong et al., 2013; Ghodrati et al., 2017) and direction of motion (Hu et al., 2000; Shou et al., 1995; XU et al., 2002) have been reported in primates and carnivores. Their functional role, however, remains unclear.

The occurrence of these cells suggests that some cells in primary visual cortex might inherit their tuning from the LGN rather than creating it de novo from untuned thalamic input. This hypothesis will be discussed in more detail in the next section.

1.3 THE VISUAL CORTEX

The neocortex is organized in six layers of sparsely interconnected excitatory pyramidal cells which make up the majority of cortical neurons. The neurons in the deeper layers mainly target subcortical areas while those located more superficially in layers 2/3 and 4 have intracortical axonal targets (Jabaudon, 2017). Neurons in layer 4 are the main targets of sensory input from first order thalamic nuclei such as the LGN.

From layer 4, information follows two parallel pathways. Despite organizational differences between rodents and “higher mammals” and even between cat and monkey or among primates, there is a general consensus that the fundamental properties of primary visual cortex (V1) apply to primates, carnivores and rodents alike. These include the existence of simple (linear) and complex (nonlinear) cells, the structure of spatial receptive fields determined by the apposition of an on and an off region and selective responses to oriented edges. These properties, initially described in cats and primates by Hubel and Wiesel (Hubel and Wiesel, 1959), have later been confirmed in mouse as well (Dräger, 1975; Huberman and Niell, 2011; Niell and Stryker, 2008).

The cells in the primary visual cortex exhibit functional properties that are more varied and complex than those of their feedforward input. The relative contribution of different sources of inputs will be discussed next.

1.3.1. Thalamocortical (feedforward) connectivity

The current understanding of thalamocortical connectivity is based on studying the transformation of single-cell receptive fields between LGN and cortex. The geniculate circular center-surround configuration is replaced by a more elongated shape with two (or more) separate on and off subfields lying parallel to each other (Hubel and Wiesel, 1959, 1962). In the classic feedforward model proposed by Hubel and Wiesel for the emergence of cortical receptive fields, simple cell receptive fields result from the convergence of geniculate inputs with spatially segregated RFs aligned in visual space (Hubel and Wiesel, 1962), as shown below in Figure 2.

A number of experimental observations support this model. Both LGN and V1 contain retinotopic maps of visual space and thalamocortical connections are retinotopically matched with high fidelity. The wiring specificity of LGN-V1 layer 4 pairs is governed by receptive field (RF) spatial overlap. The probability of connections strongly depends on the overlap between the center of a geniculate cell and a simple cell subfield of the same sign (Alonso et al., 2001; Chung and Ferster, 1998; Clay Reid and Alonso, 1995; Ferster, 1992; Reid and Alonso, 1996; Sedigh-Sarvestani et al., 2017). Furthermore, mouse layer 4 neurons receive thalamic input with spatially offset yet overlapping on and off receptive fields, as predicted by Hubel and Wiesel (Lien and Scanziani, 2013).

The response to oriented edges is a well-established property of cortical neurons which has been used extensively to study cortical computations, as it was believed for a long time to only arise in the cortex. Although it is now known that this property is present in a subset of both retinal and geniculate neurons (see previous sections), cortical orientation selectivity appears to mainly be derived from the structure of the cortical RFs, specifically the relative position of their on and off subfields (Lien and Scanziani, 2013).

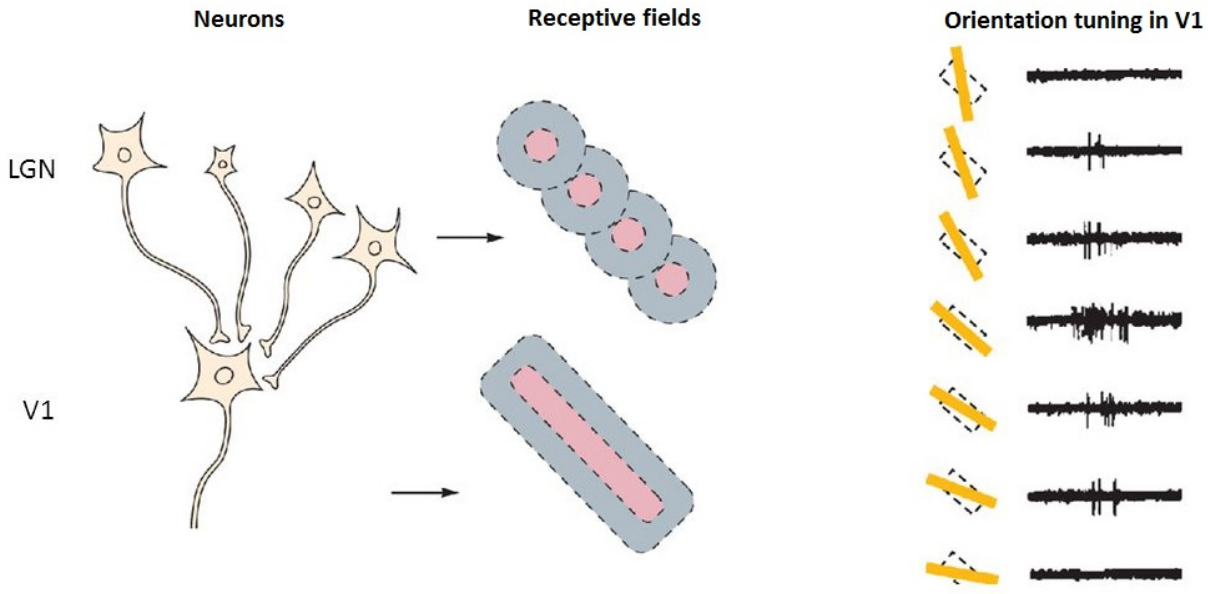

Adapted from Kandel et al. *Principles of neuroscience*

Figure 2 | Convergence of geniculate inputs onto V1 pyramidal cells

Several LGN cells with aligned and partly overlapping RFs converge their axonal projections onto one postsynaptic cortical pyramidal neuron. The arrangement of the geniculate on and off subfields generates the cortical RF structure with separate elongated on and off subfields. The position of the subfields relative to each other determines the orientation selectivity of the neuron.

The sharp tuning of the layer 4 population strongly suggests that its orientation tuning likely emerges from the combined input of all presynaptic LGN cells and is further shaped by local interactions. Intracortical interactions could also account for some of the response properties of simple cells that are at odds with a purely feed-forward model, such as contrast invariant tuning or cross-orientation suppression, which can be explained by lateral inhibition models (Priebe and Ferster, 2012).

In primate and carnivore species, neurons with similar feature preference are clustered in so-called orientation columns. These are discrete radial regions spanning the entire cortical depth, comprised of neurons responding to the same orientation (Hubel and Wiesel, 1962; Mountcastle, 1957). Across the cortical surface there is a smooth progression of the orientation preference domains

which gives rise to an orientation map. Only at specific points called “pinwheel” centers, where several orientation domains converge, the continuity is broken and neighboring neurons are selective for a wide range of orientations (Bartfeld and Grinvald, 1992; Bonhoeffer and Grinvald, 1991; Maldonado et al., 1997).

Rodents, on the other hand, exhibit a scattered “salt-and-pepper” organization (Ohki et al., 2005), whereby neurons with various response properties are spatially intermixed such that neighboring neurons can have dramatically different orientation selectivity. The same arrangement has been observed in the squirrel, a highly visual mammal (Van Hooser et al., 2005), which suggests that this organization is likely to reflect cortical size constraints rather than decreased visual acuity (Chklovskii and Koulakov, 2004).

1.3.2 Local connectivity (intracortical connections)

Excitatory input to cortical neurons arrives from two sources, thalamic and cortical. Their contribution to shaping sensory tuning properties is still not very well understood. While LGN input is thought to represent only 5-10 % of all excitatory synapses onto a layer 4 cell (Binzegger et al., 2004), in mice, it was estimated that about a third of the total excitation layer 4 cells receive is accounted for by thalamic inputs (Lien and Scanziani, 2013). The same study suggested that a main role of cortical inputs might be to amplify tuned thalamic excitation.

Other studies also provide evidence that intracortical (local) connections amplify layer 4 input without changing its tuning properties (Lien and Scanziani, 2013; Yoshimura et al., 2005). Therefore, local networks of interconnected cells should receive thalamocortical projections carrying similar visual information. This prediction was confirmed by data revealing the relationship between feedforward input and local connectivity: interconnected local networks also share common feedforward input from the thalamus (Yoshimura et al., 2005). This is true not only in L4 but also applies to connectivity from L4 to L2/3, connections being more often formed between cells sharing common thalamic input (Morgenstern et al., 2016; Yoshimura et al., 2005).

In layer 2/3, neurons with similar feature selectivity preferentially connect to each other, forming local subnetworks (Ko et al., 2011). More recently it has been shown that the probability of two neurons to share a connection is strongly dependent on the spatial overlap of their receptive fields. Furthermore, the reciprocity and strength of these connections are governed by the same rule

(Cossell et al., 2015), with larger synapses between functionally similar cells (Lee et al., 2016). Although less numerous, strong connections provide highly tuned excitation and make the main contribution to the feature selectivity of a given neuron. This connectivity pattern can provide robustness against noise and amplify relevant signals, thus strengthening the efficiency of thalamic input as well as information transmission to downstream targets (Cossell et al., 2015; Lien and Scanziani, 2013).

Substantial connectivity also exists among neurons with different feature preference, however, these connections contribute a smaller fraction of the total excitation in the L2/3 network. These inputs may be involved in behaviorally relevant local contextual interactions or provide a basis for plasticity (Cossell et al., 2015; Harris and Mrsic-Flogel, 2013).

In mammals with orientation columns this local wiring specificity can arise from spatial organization alone, however the presence of a similar principle in rodent visual cortex where cells with different functional properties are intermingled confirms that fundamental features of cortical organization seem to be preserved across species.

How could this specific connectivity arise? Spike-timing dependent plasticity enables inputs that match the activity of the postsynaptic cell within a small window of time to be strengthened, while non-synchronised inputs will be weakened. Therefore, the pattern of local connectivity observed in cortical networks could be explained by basic rules of plasticity which will facilitate connections between cells tuned to similar or commonly co-occurring features based on their synchronous firing, as postulated by Hebb's rule.

Alternatively, cortical connections might precede and instruct the acquisition of the cell's feed-forward input and therefore its functional properties. Neurons born from divisions of a common progenitor cell have indeed been shown to be more likely to share synaptic connections and orientation preference than unrelated cells (Li et al., 2012; Ohtsuki et al., 2012; Yu et al., 2012). However, the relationship between cortical connectivity and visual feature preference has been shown to be weak at eye opening and becomes stronger after visual experience.

Individual neurons therefore seem to acquire their stimulus selectivity early in development, before the onset of sensory experience, by selecting feedforward input. In contrast, recurrent connections only mature later (Ko et al., 2013). This indicates that feedforward input leads to the

formation of functionally specific subnetworks by refining pre-existing connectivity through activity-dependent mechanisms.

1.3.3 Inhibitory connectivity

In contrast to pyramidal cells which are sparsely interconnected, the largest inhibitory cell class, fast-spiking parvalbumin (PV) interneurons (Markram et al., 2004), form very dense and strong connections within local circuits (Thomson and Lamy, 2007; Yoshimura and Callaway, 2005) and receive local as well as strong feedforward input (Swadlow, 2003; Yoshimura and Callaway, 2005). They target the somata and proximal dendrites of excitatory cells and other PV neurons alike providing powerful yet short-lived inhibition (Beierlein et al., 2003).

Consistent with the hypothesis of local unselective pooling of excitatory inputs (Bock et al., 2011), PV neurons in species with orientation columns are found to exhibit a stronger stimulus preference (Sedigh-Sarvestani et al., 2017) compared to PV cells in rodent cortex which are generally more broadly tuned (Kerlin et al., 2010; Niell and Stryker, 2008). Furthermore, network co-activation patterns indicate that recurrent connectivity drives activity more strongly than visual stimulation in PV cells, as would be expected from dense connections with diverse pyramidal cells (Hofer et al., 2011). Nevertheless, reports of selective visual responses of PV neurons in these species exist (Runyan et al., 2010), suggesting some degree of fine-scale specificity generated by sampling excitatory input from mutually connected pyramidal cells (Yoshimura and Callaway, 2005).

It has been suggested that a PV-cell-dependent mechanism contributes to the sharpening of pyramidal cell tuning (Lee et al., 2012). However, PV cell activation or inactivation show little influence on the tuning properties and selectivity of neighboring neurons in visual cortex, other than an iceberg effect (Atallah et al., 2012; Wilson et al., 2012). Hence the prevalent current view is that PV neuron activity mainly serves as a global gain control mechanism, scaling the overall activity of the local network they belong to (Pouille et al., 2009; Xue et al., 2014).

Somatostatin (SOM) neurons are typically located in layers 2-6 and preferentially target apical dendrites of pyramidal neurons as well as PV cells. They have dense axonal arborizations in layer 1 and in the same layer as their somata. Based on their anatomical and physiological properties, it has been suggested that this class of interneurons is involved in feedback inhibition (Ma et al., 2010; Silberberg and Markram, 2007; Xu and Callaway, 2009). Superficial SOM neurons differ

from PV neurons by receiving predominantly lateral inputs from within layer 2/3 and much less feedforward input from layer 4 (Xu and Callaway, 2009). They are believed to at least partly mediate the cortical component of surround suppression (Adesnik et al., 2012).

This phenomenon is characterized by an inhibitory influence exerted by stimuli whose size exceeds that of a neuron's classical receptive field and was first characterized by Hubel and Wiesel (Hubel and Wiesel, 1968). More recently identified in mouse V1 (Van den Bergh et al., 2010), its presence in the retina and the thalamus indicates that it is likely partially inherited from subcortical processing. A SOM-dependent contribution of cortical surround suppression is supported by studies showing that SOM interneurons in mouse V1 lack surround suppression and that surround suppression in layer 2/3 pyramidal neurons is decreased when SOM neurons are silenced (Adesnik et al., 2012; Nienborg et al., 2013).

Vasoactive intestinal polypeptide (VIP)- expressing neurons comprise only 1–2% of all cortical cells (Yavorska and Wehr, 2016). While they provide weak inhibition to PV cells their vertical axonal projections enable them to strongly target SOM cells in layer 2/3, and thus modulate the activity of the local population of pyramidal cells by forming disinhibitory circuits (Pfeffer et al., 2013; Pi et al., 2013). They are believed to receive top-down input from outside the visual cortex, which might provide associative and behavioral context information (Fu et al., 2014; Kepecs and Fishell, 2014; Pi et al., 2013).

1.3.4 Long range connectivity

Long range inputs can originate from multiple sources, including horizontal connections from within the same cortical area, feedback projections, as well as feedforward connections. This heterogeneous group is characterized by the distance the axonal projections travel to reach their synaptic partners, which exceeds the few hundred micrometers boundary typically assigned to the local network space (likely matching the size of one orientation column).

Synaptic partners from beyond the local network make up a substantial fraction of the total input a cortical neuron receives (Binzegger et al., 2004; Stepanyants et al., 2009) and, in sensory cortices, many of these inputs originate from neurons representing distant topographic positions (Angelucci et al., 2002; Gilbert and Wiesel, 1989; Rockland and Lund, 1983).

Long-range lateral projections mainly arise from pyramidal cells and can span millimeters parallel to the cortical surface (Gilbert and Wiesel, 1983; Rockland and Lund, 1982). Previous studies in both cat and primate visual cortex have provided anatomical evidence that they form patchy terminations which preferentially link neurons located in iso-orientation columns (Bosking et al., 1997; Gilbert and Wiesel, 1989; Malach et al., 1993; Martin et al., 2014) and in some species these extend along the axis of the retinotopic map that corresponds to their preferred stimulus orientation (Bosking et al., 1997; Schmidt et al., 1997; Sincich and Blasdel, 2001).

In tree shrew visual cortex, where they are formed primarily by the axon collaterals of layer 2/3 pyramidal neurons, horizontal connections exhibit specificity for the axis of projection. Axons extend for longer distances, and form more terminal boutons, along the axis that matches the preferred orientation of their origin site. On a smaller distance scale, the pattern of connections is much less specific, with boutons found along every axis, contacting sites with a wide range of preferred orientations. (Bosking et al., 1997).

In species such as tree shrew and ferret, where there is a marked difference in the tuning between different layers, this connectivity structure could contribute to the sharper tuning observed in layer 2/3 compared to layer 4 (Chapman and Stryker, 1993; Humphrey and Norton, 1980).

Layer 6 neurons of cat visual cortex provide an example for the contribution of long range connections to cortical computations. These cells are characterized by long receptive fields, which are formed by pooling information from regions of cortex representing large parts of the visual field. The axons of layer 5 pyramidal cells project over long distances within layer 6 and this extensive convergence of projections from layer 5 to layer 6 is responsible for generating the characteristic receptive fields (Bolz and Gilbert, 1989). Moreover, it appears that this convergence follows a specific pattern, whereby these projections have a collinear arrangement.

Horizontal connections have also been proposed to mediate particular receptive field surround effects, as will be discussed in the following section.

In species with cortical columns the specificity of long-range projections suggested by their projection patterns is reminiscent of the organization of local networks. On a single cell level, however, the precise relationship between a neuron’s visual feature preference and those of its

long range inputs remains unknown. Furthermore, whether these connectivity rules also apply to non-columnar species has not been investigated.

1.3.5 Connectivity and visual contextual interactions

Any given neuron in the primary visual cortex responds with action potential firing only to stimulation of its receptive field, which is restricted to a small segment of the overall visual scene. Most objects, however, extend over much larger areas of the visual field. The visual system must therefore combine information arising from different parts of the visual field, giving rise to contextual effects whereby the perception of one stimulus can be differently influenced by the presence of other stimuli at different positions of the visual field.

The influence contextual information can exert on the activity of visual cortex neurons from beyond their classical receptive field might lead to various visual perceptual phenomena. So called receptive field surround effects are for instance thought to contribute to perceptual phenomena such as contour integration or figure-ground segregation. Visual stimuli placed outside a neuron's receptive field can either suppress or enhance responses of this neuron to stimuli within its receptive field.

The main surround effect that has been described is surround suppression. In this case, neurons decrease their firing in the presence of a stimulus centered on their receptive field but whose size exceeds it. Although this effect is already present in the retina and thalamus (Alitto and Usrey, 2008, 2015; Bonin et al., 2005), some studies suggest that the cortex also has a contribution (Bolz and Gilbert, 1986; Ozeki et al., 2009). SOM-positive interneurons have been identified as being at least partly responsible for the cortical component of surround suppression (Adesnik et al., 2012). Additionally, recent results suggest involvement of excitatory feedback from higher visual areas and from superior colliculus (A.Heimel unpublished).

Facilitating effects have also been described in both cats and primates. These effects often exhibit axial specificity. This means surround stimuli have a stronger influence in regions of visual space located along the axis of the neuron's preferred orientation than along the orthogonal axis (Kapadia et al., 1995; Nelson and Frost, 1985). Specifically, in macaque visual cortex the addition of a stimulus outside the receptive field enhances neuronal responses if this stimulus matches the preferred orientation and is collinear with the stimulus within the receptive field (Kapadia et al.,

1995). This process occurs in a strongly context-dependent manner, as the spatial separation of the stimuli determines the degree of facilitation and non-collinearity will suppress or only weakly facilitate the responses (Cannon and Fullenkamp, 1991; Grinvald et al., 1994; Kapadia et al., 1995; Levitt and Lund, 1997; Sengpiel and Blakemore, 1996).

Human psychophysics experiments provide additional proof of this effect. In contour detection tasks, the performance of human observers is improved when the segments composing the contour are collinear with the path of the contour rather than when they are aligned orthogonal to the path. When identifying a contour among an array of distractors, performance is dependent on both the orientation and position of the elements (Field et al., 1993).

These observations indicate that connectivity between neurons that underlie such surround effects should be specific, requiring not only similar orientation tuning of interacting neurons, but also receptive fields centered along the same axis (Ito and Gilbert, 1999; Kapadia et al., 1995, 2000; Polat and Norcia, 1998).

While the exact mechanisms mediating these effects have as of yet not been fully elucidated, based on anatomical data and temporal and spatial properties of the surround effects multiple mechanisms have been proposed including recurrent horizontal connections or feedback from extrastriate cortex acting via local inhibitory neurons (Chisum and Fitzpatrick, 2004; Hess and Field, 1999; Loffler, 2008; Polat and Sagi, 1993; Wilson and Wilkinson, 2002).

Long-range lateral connections could provide a potential circuit substrate for collinear facilitative effects, which might underlie the perception of continuity in visual scenes. This hypothesis is supported by anatomical data showing that axons forming long range horizontal connections have a collinear arrangement, projecting along the axis of the preferred orientation of their origin site (Bosking et al., 1997; Schmidt et al., 1997; Sincich and Blasdel, 2001).

Thus, specific organization of horizontal connections seems well suited for mediating contour detection as well as other related Gestalt phenomena such as perceptual filling in or object grouping.

1.3.6 Single-cell signal integration

At the population level, different firing strategies - for instance sparse or dense AP firing, sustained or phasic responses, bursting or tonic firing - allow neurons to expand their coding power and endows them with the ability to rapidly, accurately and flexibly respond to the environment.

Nevertheless, the spiking activity of any given neuron ultimately abides by an "all-or-none" law. Simply put, a neuron can either respond to stimulation with an action potential of standard amplitude and length or do nothing. As such, it falls onto each individual cell to perform input-output transformations that enable it to integrate a various array of information arising from thousands of synapses and generate an adequate response under various conditions.

Initially it was thought that neurons simply sum their inputs linearly to generate spikes, but it has become clear that this process is not nearly as straightforward. Most synapses are formed on dendrites, and these often play a critical role as distinct computational units of a neuron.

Decades of study on dendritic integration revealed various linear and nonlinear processes that govern input integration (Stuart and Spruston, 2015). The complex geometry of the dendritic tree, combined with its passive and active properties, enable multiple types of dendritic electrical signals which allow neurons to perform a wide range of operations on their inputs (Lien and Scanziani, 2013; Yoshimura et al., 2005). Consequently, many studies have aimed to define the array of computations dendrites can perform.

In vitro studies have been instrumental for the initial characterization of dendritic electrical properties. The array of channels and receptors dendrites possess and their differential distribution depending on cell type and dendritic arbor location represent the building blocks of a neuron's input integration capacity (Migliore and Shepherd, 2002). In pyramidal neurons, the key players for dendritic activity are Na^+ and Ca^{2+} voltage-dependent channels, together with NMDA receptors (Stuart and Sakmann, 1994; Stuart and Spruston, 2015).

Passive integration is largely determined by the interaction between the amplitude and frequency of the EPSPs generated by synaptic stimulation and the voltage attenuation along dendrites. Active integration, on the other hand, provides additional computational dimensions through the interplay of synaptic input and back propagating action potentials (bAP) or locally generated activity such

as dendritic spikes. The latter can be generated at different locations on the dendritic tree, and can be mediated by different channel types. The ability of dendritic spikes to propagate to the soma varies accordingly (Schiller et al., 1997, 2000; Stuart et al., 1997). Regardless, they can all exert a substantial influence on action potential generation (Palmer et al., 2014; Stuart et al., 1997; Williams and Stuarty, 1999) and often occur in concert with bAPs.

As the name suggests, bAPs are waves of activity generated at the axon initiation segment which spread into the dendrites, often attenuating with distance (Stuart et al., 1997). Pairing weak synaptic stimulation with bAPs can lower the threshold for the generation of dendritic calcium spikes (Matthew E. Larkum et al., 1999; M E Larkum et al., 1999), leading to AP burst firing. Conversely, propagation of bAPs into the dendritic tree can reduce the probability of subsequent dendritic sodium spike generation (Golding and Spruston, 1998).

Active integration mechanisms allow differential integration across the dendritic arbor, supporting the discrimination of different input sequences in various spatial distributions on single branches and maximizing the efficiency of distal synaptic inputs. On distal dendritic segments, inputs require less synchrony and are amplified more strongly than on proximal segments, where integration is more linearly and high synchrony is required for summation (Branco et al., 2010; Branco and Häusser, 2011). As a result, neurons are able to use multiple integration rules on specific subsets of inputs.

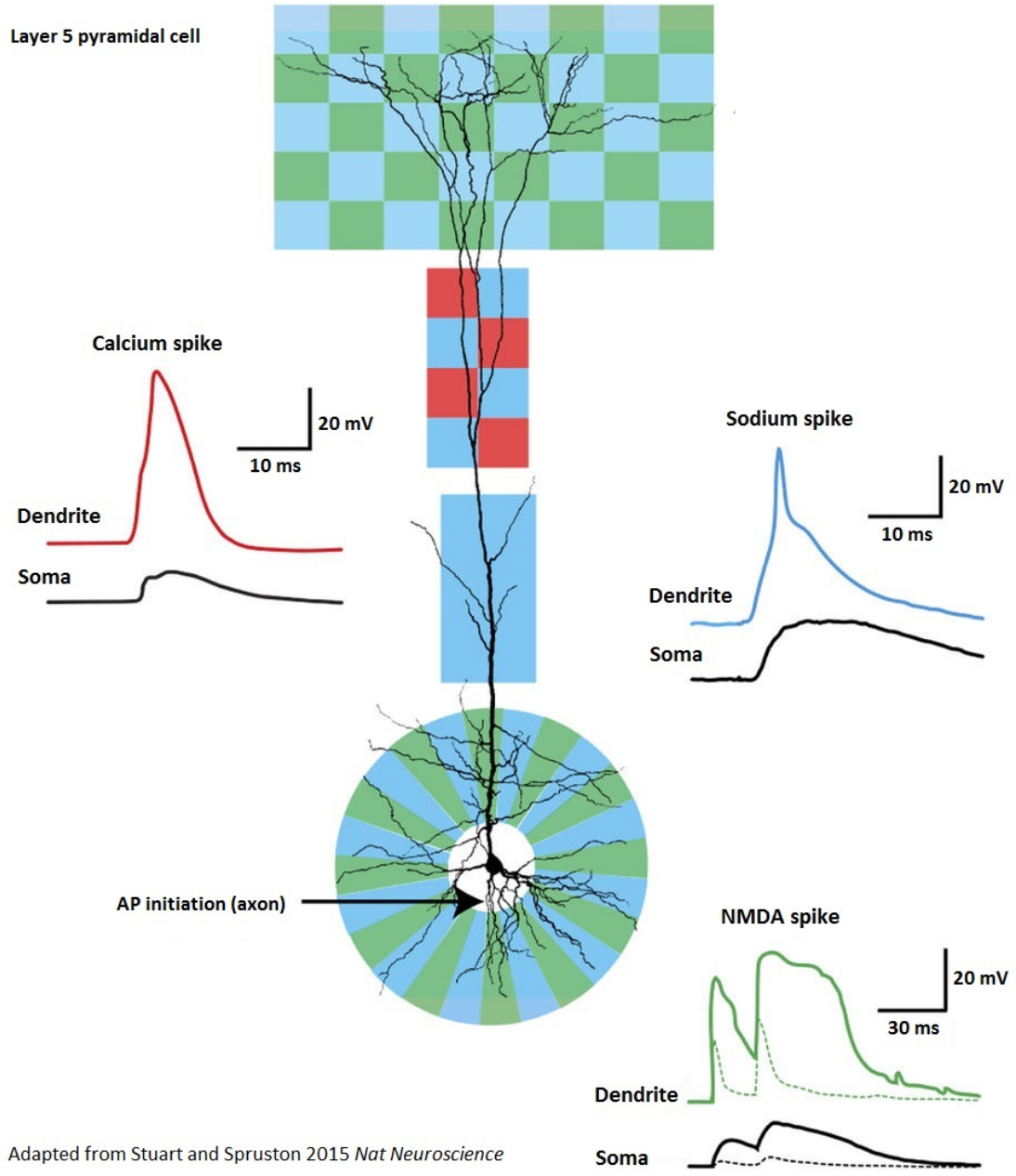

Figure 3. Locally generated dendritic activity

Pyramidal cells can combine and implement different strategies at different locations of the dendritic tree to overcome physical limitations and improve signal propagation to the soma. Dendritic sodium (blue), calcium (red) and NMDA (green) spikes evoked by synaptic stimulation are generated in distinct regions of the dendritic tree, as indicated by the superimposed colored boxes and circles. The black traces show somatic activity during simultaneous recordings. Dotted lines indicate the effect of blocking NMDA receptors.

Similar active mechanisms have also been confirmed in vivo, where they have been implicated in a multitude of physiologically and behaviorally relevant computations (Helmchen et al., 1999; Hirsch et al., 1995; Jagadeesh et al., 1992; Svoboda et al., 1999; Waters et al., 2003).

In vivo recordings in multiple sensory areas and across cortical layers have provided evidence for a role of active dendritic signals in sensory processing and different aspects of behavior. Layer 2/3 distal dendrites show patterns of dendritic activity brought about by a mixture of sodium, calcium and NMDA dendritic spikes which are thought to enhance stimulus selectivity (Smith et al., 2013).

NMDA spikes in tuft dendrites of neurons in the same layer have been shown to influence action potential generation (Palmer et al., 2014). In layer 5, apical dendrites of pyramidal neurons act as coincidence detectors using sustained dendritic Ca events to integrate sensory and motor signals (Xu et al., 2012). Dendritic NMDA spikes in layer 4 spiny stellate cells help integrate thalamocortical and corticocortical inputs and contribute markedly to somatic tuning (Lavzin et al., 2012). In contrast, other studies have failed to detect nonlinear dendritic integration. Somatic recordings from layer 2/3 neurons in binocular visual cortex indicate linear or sublinear integration in both anesthetized and awake animals (Longordo et al., 2013; Zhao et al., 2013b).

Together, these studies indicate that a range of integration modes (linear, supralinear and sublinear) can occur in the dendrites of layer 2/3 neurons during sensory input. Both linear (Jia et al., 2014) and supralinear integration has also been observed in layer 4 neurons in somatosensory cortex.

In order to be able to fully describe single-cell computations and to understand their contribution to overall cortical computation, a detailed description of the input itself is required. Are there rules in the organization of the input itself that can select specific integration mechanisms over others in order to make certain signals more salient?

For example, the spatial organization of inputs could have important functional implications. Co-localization could be a useful strategy for inputs carrying similar signals to increase their transmission efficiency. Some studies report a certain degree of clustering of functionally similar inputs (Kleindienst et al., 2011; Takahashi et al., 2012), while others fail to observe spatial organization of inputs with certain response properties (Chen et al., 2013; Jia et al., 2010). A certain

degree of clustering on a small scale (close-by synapses) might be expected through cooperative reinforcement of these synapses based on concomitant activation (Weber et al., 2016).

In ferret visual cortex, within the dendritic tree of a single neuron, some branches exhibit increased clustering, while others show no obvious spatial arrangement of inputs. The relative number of tuned branches varies across neurons and is correlated with their degree of orientation selectivity, supporting a functional role for input clustering (Wilson et al., 2016).

1.3.7 Functional synaptic plasticity

A crucial factor for setting up and refining neuronal circuits is synaptic plasticity, which can be described as a complex interplay between associative (most commonly Hebbian) and homeostatic plasticity mechanisms. The former is closely linked to neuronal activity and reflects correlated firing between the pre and postsynaptic cells through changes in connection strength (Hebb 1949). The latter acts as a counterweight, ensuring network stability by preventing hypo or hyper excitability (Renart et al., 2003).

Briefly, homeostatic plasticity is dependent upon cellular-level mechanisms that regulate excitability. The total synaptic strength must be continuously regulated to counterbalance changes induced by associative plasticity (Keck et al., 2017). This regulation is achieved by multiple mechanisms, such as changes in quantal amplitude, release, number of receptors and even input resistance (Keck et al., 2013; Turrigiano and Nelson, 2004). Often these mechanisms globally scale synaptic strength, which allows the strength ratios between different synapses, as determined by Hebbian plasticity, to be preserved (Turrigiano, 2011; Turrigiano and Nelson, 2004).

Hebbian plasticity would be well suited to play an instrumental role for the specific connectivity we witness as a re-occurring wiring principle, ensuring that “cells that fire together wire together” (Lowel and Singer, 1992). It strongly but non-exclusively relies on timing and can be dramatically shaped by several factors including firing rate, dendritic depolarization and neuromodulation (Feldman, 2012).

Simultaneous or rapid sequential activation of two interconnected neurons induces changes in the strength of the synapses between them. The timing and order of pre- and postsynaptic activity are the main factors underlying the occurrence, magnitude and direction of plasticity (Debanne et al.,

1994, 1997; Levy and Steward, 1983; Markram et al., 1997). Long term potentiation (LTP) occurs if a presynaptic spike precedes a postsynaptic one within a narrow window of 20 ms. Conversely, long term depression (LTD) requires the opposite order in a slightly longer time window (Bi and Poo, 1998; Markram et al., 1997).

Consequently, Hebbian spike timing-dependent plasticity (STDP) strengthens inputs that are synchronous with or lead to postsynaptic firing and depresses inputs that do not succeed the spike or are non-synchronized. Not all associative plasticity is, however, timing dependent: sufficiently high or low firing frequencies can also induce LTP or LTD, respectively.

The molecular players for plasticity at glutamatergic synapses are most often NMDA receptors, well suited to act as molecular coincidence detectors as they conduct current only when glutamate is bound and the postsynaptic neuron is depolarized (Lüscher and Malenka, 2012). Correlated presynaptic release and postsynaptic depolarization trigger calcium influx through postsynaptic NMDA receptors and voltage-dependent calcium channels.

The concentration of calcium determines whether the synapse is going to be potentiated (high and brief), depressed (moderate and sustained) or if nothing will happen (low) (Feldman, 2012; Lisman, 1989; Yang et al., 1999). As a consequence, AMPA receptors will be additionally inserted or removed at the synaptic site (Malinow and Malenka, 2002). An alternative pathway for LTD requires mGlu and cannabinoid signaling to decrease the release probability on the presynaptic terminal (Sjöström et al., 2003).

The timing dependence of plasticity requires electrical dendritic signaling, whose dynamics are essential (Magee and Johnston, 1997). As mentioned previously, somatic action potentials back propagate decrementally to the dendrites (Spruston, 2008). For LTP to occur, signal enhancement is required in the form of additional depolarization (Sjöström et al., 2001; Sjöström and Häusser, 2006). This can be provided by EPSPs generated shortly before the bAP reaches the dendritic location of the synapse (Stuart et al., 1997).

Because of the decremental backpropagation of APs, spatial gradients are created and other strategies need to be employed at distal synapses (Froemke et al., 2005; Kampa et al., 2007; Spruston, 2008), namely local dendritic calcium spikes (Golding et al., 2002; Gordon et al., 2006).

At the single-cell level these mechanisms enable selective reinforcement of relevant inputs and loss of irrelevant ones and the specific spatial arrangement of inputs. At the network level plasticity mechanisms provide an ideal basis for experience-dependent refinement of cortical connectivity.

1.4 AIMS OF THE THESIS

The last decade(s) of vision research have brought about a great deal of progress in our knowledge of visual processing and cortical computations in general. During this time, it has become evident that organization principles play a key role. Consequently, the term “functional organization” was born, the relationship between connectivity and functional properties both at the level of single cells and neuronal populations.

Studying the functional organization of local networks revealed a high degree of functional specificity in synaptic connections, which might be important for maintaining the high selectivity of visual cortex neurons. The exact organization principles of long range connectivity, however, remain as yet unknown. Previous anatomical data indicates that axonal long range projections also show specificity by targeting areas with feature preferences similar to those of the areas they originate from, but the precise connectivity pattern between individual neurons remains unexplored.

In this study, we used in vivo two photon calcium imaging in mouse primary visual cortex to investigate the functional properties and organization of long-range excitatory synaptic inputs to V1 neurons and characterize the relationship between visual feature preference and connection specificity.

2. Synaptic organization of visual space in primary visual cortex

2.1 INTRODUCTION

Understanding the mechanisms of sensory processing requires uncovering the precise relationship between synaptic connectivity and function of neurons in cortical circuits. Local connectivity between neurons follows certain rules. For example, neighbouring L2/3 pyramidal neurons in rodent visual cortex preferentially connect if they receive common synaptic input (Ko et al., 2011; Yoshimura et al., 2005) or if they respond to similar stimulus features within their RFs (Cossell et al., 2015; Lee et al., 2016; Wertz et al., 2015a). Additionally, how a sensory stimulus is processed and perceived depends on the surrounding visual scene. In the visual cortex, contextual signals can be conveyed by an extensive network of intra- and inter-areal excitatory connections that link neurons representing stimulus features separated in visual space (Binzegger et al., 2004). However, the rules of long-range synaptic connectivity remain poorly understood. A substantial fraction of the synaptic inputs a cortical neuron receives originate outside its local network (Markov et al., 2011) and, in sensory cortices, many inputs stem from neurons representing distant topographic positions (Rockland and Lund, 1983; Stepanyants et al., 2009). Long-range lateral projections in cat and primate primary visual cortex (V1) preferentially (but not exclusively) link orientation columns with similar preferences (Angelucci et al., 2002; Gilbert and Wiesel, 1989; Malach et al., 1993; Rockland and Lund, 1983), and in some species these extend along the axis of the retinotopic map that corresponds to their preferred stimulus orientation (Angelucci et al., 2002; Bosking et al., 1997; Martin et al., 2014). While these studies reveal a degree of functional specificity of long-range projections, at least in animals with cortical columns, it is still unclear what repertoire of visual information a single neuron receives from the extended visual scene, and how this visual input relates to a neuron's visual feature preference. This knowledge is important for uncovering the circuit mechanisms of contextual processing and related perceptual Gestalt phenomena, such as integration of contours and object grouping in the visual environment (Schmidt et al., 1997; Sincich and Blasdel, 2001).

2.2 METHODS

2.2.1 Animals and surgical procedures

All experimental procedures were carried out in accordance with institutional animal welfare guidelines, and licensed by the Veterinary Office of the Canton of Basel, Switzerland. Experiments in this study were performed in 31 male and female C57BL/6 mice, aged 2-4 months (spine RF mapping: 21 mice; neural population RF mapping: 7 mice; somatic and dendritic RF mapping: 3 mice).

Prior to surgery, the animals were injected with dexamethasone (2 mg kg-1), atropine (0.05–0.1 mg kg-1) and analgesics (carprofen; 5 mg kg-1). General anaesthesia was induced with a mixture of fentanyl (0.05 mg kg-1), midazolam (5.0 mg kg-1), and medetomidine (0.5 mg kg-1). Viral injection and window implantation were performed as described previously (Chen et al., 2013; Holtmaat et al., 2009). Briefly, a small craniotomy was made over right V1, and for spine imaging 90-120 nl of a mixture of highly diluted AAV9.CaMKII.Cre (1:20000) and AAV2/1.Syn.Flex.GCaMP6s.WPRE or AAV2/1.CAG.Flex.mRuby2-2A-GCaMP6s.WPRE was injected using a glass pipette and a pressure injection system (Picospritzer III, Parker) to achieve sparse labelling of 5-10 pyramidal cells. For population imaging 90 nl of AAV2/1.Syn.Flex.GCaMP6s.WPRE mixed with AAV9.CaMKII.Cre (1:1000) or AAV2/1.Syn.GCaMP6s.WPRE were injected instead. The skin was sutured shut after the injections. Two to four weeks after virus injection a craniotomy of 4 mm diameter was made over right V1. The craniotomy was sealed with a glass coverslip and cyanoacrylate glue (UltraGel, Pattex) and a head plate was attached to the skull using dental cement (Heraeus Sulzer or C&B). Animals were given antibiotics and analgesics (enrofloxacin 5 mg kg−1, buprenorphine 0.1 mg kg−1) at the end of surgeries and repeatedly during recovery. Imaging started earliest 4 days later.

2.2.2 Two-photon calcium imaging and visual stimulation

For imaging, mice were lightly anesthetized with chlorprothixene (1 mg kg-1) and isoflurane (0.4–0.8% in 1:1 mixture of N_2O and O_2). Atropine was given to slightly dilate the pupil and reduce mucus secretion. Eyes were covered with eye ointment (Maxitrol). The ointment was reduced to a thin layer during imaging on the eye contralateral to the imaged hemisphere to keep it moist. The ipsilateral eye remained covered. Rectal temperature was kept constant at 37 °C via a heating pad

(DC Temperature Controller, FHC). The pupil position was monitored throughout each experiment.

Imaging was performed using a commercial resonance scanning two-photon microscope (B-Scope; Thorlabs) and a Mai Tai DeepSee laser (SpectraPhysics) at 930 nm with a 40× water immersion objective (0.8 NA; Olympus). Images of 512 × 512 pixels with fields of view of ~30 × 30 μm (dendritic imaging) or ~450 × 450 μm (neuronal population imaging) or ~250 × 250 μm (soma and dendrite imaging) were acquired at a frame rate of 15 Hz using ScanImage 4.2 (Pologruto et al., 2003). For population imaging experiments and comparison of dendritic and somatic calcium signals, a piezo z-scanner (P-726.1CD, Physik Instrumente) was used to rapidly move the objective in the z-axis and acquire 2 image planes simultaneously at 15 Hz frame rate, separated by 10 - 50 μm in depth. The power supply of the monitor backlight was controlled using a custom-built circuit (Leinweber et al., 2014) to present visual stimuli only in-between the scanning of two subsequent lines.

Visual stimuli were generated in Matlab using Psychophysics Toolbox (Brainard, 1997) and presented on a calibrated LCD monitor (60 Hz refresh rate) positioned 20 cm from the left eye at approximately 45° to the long axis of the animal, covering ~110° × 80° of visual space. At the beginning of each experiment, the appropriate retinotopic position in visual cortex was determined using small grating stimuli at 12 positions arranged in a 4 x 3 grid. The monitor was positioned such that the preferred retinotopic position of the imaged neurons was roughly centred on the screen.

Receptive field mapping stimuli consisted of black (<0.05 cd m-2) and white (43 cd m-2) squares of 8° × 8° on a grey background (23 cd m^{-2}). The squares were presented one at a time and in random order at one of 120 positions (12 × 10 matrix covering a total area of 96° × 80°; each position was repeated 12 times). The presentation rate was ~1.7 Hz and the duration of each stimulus was ~0.4 s, followed by 0.2 s blank screen. Sinusoidal gratings (0.03 cycles per degree, measured at the shortest distance between the eye and the monitor, 2 Hz, 100% contrast) drifting in 12 different directions for 1.5 s were presented randomly and were interleaved with a grey screen (~2 s) between grating presentations. Each grating direction was repeated 10-12 times.

To measure visually-evoked calcium signals in dendritic spines, individual neurons in layer 2/3 were selected for imaging based on several criteria: the baseline fluorescence of dendritic branches was high enough for dendritic spines to be visible, the nucleus was devoid of GCaMP6 expression, and cells exhibited selective visual responses and defined spatial receptive fields. After each recording, the focal plane and imaging position was checked and realigned with the initial image plane if necessary, and dendrites were carefully monitored for indications of photo damage. *Z*-stacks of individual cells and their dendritic arbours were acquired after dendritic imaging by averaging 20 frames per plane using 1-µm *z*-steps. Each animal was imaged repeatedly over the course of 4-5 weeks.

2.2.3 Data analysis

All analyses were performed in Matlab (MathWorks). Image stacks were registered (Guizar-Sicairos et al., 2008) to a 200-frame average to correct for x-y motion. Spine, dendrite and single-cell soma regions of interest (ROIs) were drawn manually. For population imaging data, a semi-automated algorithm was used to detect cell outlines, which were subsequently confirmed by visual inspection. This algorithm was based on morphological measurements of cell intensity, size and shape. The cell-based ROIs were then eroded to reduce the influence of the neuropil signal around the cell bodies.

All pixels within each ROI were averaged to yield a time course. Calcium $\Delta F/F_0$ signals were obtained by using the median between the 10th and 70th percentile over the entire fluorescence distribution as F_0. The $\Delta F/F$ trace was high-pass filtered at a cut-off frequency of 0.02 Hz to remove slow fluctuations in the signal. Single spine calcium signals were isolated from global dendritic signals using a subtraction procedure described previously (Chen et al., 2013) (**Fig. 2**). Dendritic signals were removed from spine signals by subtracting a scaled version of the dendritic shaft signal where the scaling factor equals the slope of a robust regression (MATLAB function 'robustfit.m'). For verification, we repeated the main analyses after selecting only those spines that showed no trial-to-trial correlation with the dendritic shaft signal after dendritic signal subtraction (77% spines, correlation coefficient not significantly different to trial shuffled controls, $P > 0.01$, Wilcoxon rank sum test; **Fig. 3**). Importantly, for spines with RFs displaced from that of the dendrite, we re-extracted RFs after removing the trials during which the dendrite was active (defined as those trials in which the activity of the dendrite exceeded the mean average activity of

all stimulus positions plus three standard deviations). 96% of spines still showed significant RFs which were highly similar to those computed from all trials and results were not changed (**Fig. 3**). A fast non-negative deconvolution was used to denoise the calcium signals (Vogelstein et al., 2010). We found no difference between data obtained from apical or basal dendrites, these were therefore combined for all subsequent analysis.

2.2.4 RF estimation

The ON and OFF subfields of spatial RFs were derived separately by analysing the responses to white and black stimulus patches, respectively. A response was defined as the mean denoised calcium signal in a window of three to five frames. Usually the first frame that reached significance over the 120 stimulus positions ($P < 0.05$, one-way ANOVA) was the first frame of the response window. In some cases, the response window was optimized through visual inspection. A one-way ANOVA across the 120 stimulus positions was then calculated for the averaged response within the defined response window. ROIs that did not pass this test for either subfield were excluded from further analysis. Raw RFs represent the mean response at each of the 12 × 10 stimulus positions. The raw RF was interpolated at 1° resolution, z-scored and smoothed with an 11° × 11° square filter. We then calculated the amount of overlap between the ON and OFF RFs as

$$\text{overlap} = \frac{ON \cap OFF}{ON \cup OFF}$$

where *ON* and *OFF* are the regions of visual space covered by ON and OFF subfields, respectively, after thresholding at 2 standard deviations above the mean. In the rare cases in which more than one region remained after this step, all but the one containing the strongest average response were removed. Thresholding of RF subfields and removal of additional subfields was only used to quantify the RF size and the degree of RF overlap. For ROIs with overlap < 0.6 we combined the two maps by scaling them according to the significance of each subfield and assigning positive values to the smoothed ON subfield and negative values to the smoothed OFF subfield. The combined smoothed RF was parameterized by fitting a two-dimensional Gabor function using the Levenberg–Marquardt algorithm. The Gabor function is described by

$$G(x', y') = Aexp\left(\frac{-x'^2}{2\sigma_x^2} - \frac{y'^2}{2\sigma_y^2}\right) cos(2\pi f x' + \varphi)$$

where

$$x' = (x - c_x)cos\theta - \big(y - c_y\big)sin\theta$$

$$y' = (x - c_x)sin\theta + \big(y - c_y\big)cos\theta$$

These equations describe an underlying two-dimensional cosine grating parameterized by θ (orientation), f (spatial frequency) and φ (phase), which is enveloped by a two-dimensional Gaussian function parameterized by A (amplitude), (c_x,c_x) (centre of the Gaussian) and σ_x and σ_y (standard deviations of the Gaussian perpendicular to and parallel to the axis of the grating, respectively).The quality of the Gabor fit was assessed evaluating the summed square of residuals (SSE, obtained from the *fit.m* function in Matlab). Only ROIs with SSE < $6.5x10^{-9}$ and a Pearson's correlation coefficient between the Gabor fit and the smoothed RF > 0.4 were included for further analyses. The Gabor fits were used to compare the amount of subfield overlap between pairs of spines (**Fig. 5**). In this case, ON subfields were defined as the region in which pixels of the Gabor fit were >20% of maximum absolute value, $max(|(Gaborfit)|)$. Similarly, OFF subfields were defined as the region in which pixels of the Gabor fit were <20% of the negative of the maximum absolute value, $-max(|(Gaborfit)|)$. The amount of overlap was defined as

$$overlap = \frac{|A \cap B|}{|A \cup B|}$$

where A and B are the regions of visual space covered by the spine A and spine B ON, OFF, or both subfields.

A pixel–to-pixel Pearson's correlation coefficient of smoothed RFs was used as a measure of RF similarity. The orientation of the RFs was obtained from the Gabor fits (variable θ from the Gabor function) and the distance between RFs was calculated from the centre between the ON and OFF subfields in the Gabor fit. Each spine RF separated by more than 30 degrees from the dendrite RF was assigned to co-axial or orthogonal visual space according to the position of its RF centre relative to the position of the dendrite RF centre and orientation (**Fig. 12a**). The co-axial space was defined as the visual space up to 45 degrees on either side of the axis extending along the orientation of the dendritic RF, running through the dendrite RF centre (also referred to as the collinear axis). Conversely, the orthogonal space was the remaining visual space, beyond 45

degrees off the dendritic RF's collinear axis (see **Fig. 12a**). Receptive field structure and size were similar between RFs in co-axial and orthogonal space as measured by σ_x σ_y of the RF Gabor fit and their ratio, the orientation of the RFs and the area and axis-length of the subfields (all P-Values > 0.1, Kolmogorov Smirnov Tests). Moreover, errors of the Gabor fits and the correlation between the Gabor fits and the raw RFs were similar (all P-Values > 0.7) and calcium responses in the two populations of spines showed similarly few co-occurring dendritic events and similarly low correlation with the dendritic calcium signal (P-Values > 0.4).

To examine the retinotopic organization of synaptic inputs onto V1 neurons (**Fig. 10**), we combined spine data from all cells with known cell body position. We correlated the relative RF positions of spines (separately for elevation and azimuth) with the location of the spine ROI in cortical space relative to the cell body on a series of axes parallel to the cortical surface spanning 360° at 1° intervals. The direction with the highest correlation between relative RF positions and relative cortical position of all spines was taken as the direction of the retinotopic gradient for azimuth and elevation, respectively. For multiple comparisons, a Kruskal-Wallis test was followed by a Wilcoxon rank-sum test. Reported P-values are Bonferroni-corrected. The same procedure was repeated after averaging the relative RF position and cortical position of all spines with significant RFs on each dendrite (**Fig. 10c**).

2.2.5 Receptive field transformation

To combine the position and orientation of all spine RFs (relative to dendritic RFs) in a common coordinate framework (**Fig. 12 b,c**), we rotated the dendritic RFs such that their orientation was vertical ($\theta = 0$) and then translated them such that their centres were aligned at the same position (**Fig. 11a**). The parameters of this transformation were then used to transform the RFs of all spines to maintain the spatial relationship of their RF to that of their parent dendrite (**Fig. 11b**) (Reid and Alonso, 1995; Cossell et al., 2015).

2.2.6 Grating responses

As a quality control for the RF fitting, the orientation preference of spine signals derived from the RF structure was compared to that inferred from drifting gratings (**Fig. 4**). The denoised calcium signal averaged over the stimulus period was taken as the response to each grating direction. Responses from different trials were averaged to obtain the orientation tuning curve. First, the

preferred orientation (θ_{pref}) of the cell was determined as the stimulus that produced the strongest response. The orientation tuning curve was then fitted, with the sum of two Gaussians centred on θ_{pref} and $\theta_{pref} + \boldsymbol{\pi}$, of different amplitudes A1 and A2, both with equal width $\boldsymbol{\sigma}$ (constrained to > 15°), and a constant baseline B. The preferred direction was adjusted by the angle at which the fitted tuning curve attained its maximum. The preferred orientation was taken as the modulus of the preferred direction to 180 degrees. The mean firing rates for the different stimulus directions were tested for differences by one-way ANOVA. Only spines or dendrites with $P < 0.01$ and R^2 for the orientation tuning curve fitting > 0.7 were included for further analysis.

2.2.7 Population RFs

The same RF mapping protocol and analysis was repeated at the population level, with the exception that the median of the responses, instead of the mean, was used to estimate the ON and OFF RFs. The cortical distance between a pair of cells was defined as the Euclidean distance between the centre of mass of their cell bodies in the imaged plane. Because the size of the imaged field of view determines the distribution of cell pair distances in the sampled population, we estimated the likelihood of finding a RF distance as the probability of a given RF distance for the sample of the cell pairs within a given range of cell pair distances using 50 μm intervals (**Fig. 8**).

2.2.8 Cell morphology

We used the Simple Neurite Tracer plugin from ImageJ to analyse the *Z*-stacks of individual cells and trace the imaged dendrites back to the cell body. We measured the distance along the dendrite between spines and the cell body after smoothing the traced skeleton with a moving average window of 4 pixels. We determined the branch order of imaged dendritic segments based on the number of bifurcations from the cell body, together with changes in branch thickness or trajectory after a bifurcation. To study the relationship between physical distance and RF properties of spines, we measured the inter-spine anatomical distances along traced dendrites making the simplifying approximation that the dendritic segment is one-dimensional rather than a tube.

2.2.9 Analysis of natural images

A set of 375 black and white images from David Attenborough's BBC documentary Life of Mammals, depicting natural scenes such as landscapes, animals or humans, of 384×208 pixels in size, was used to analyse the co-occurrence of similarly oriented edges in natural scenes. Each

image was divided in multiple sub-regions of 36 pixels, equivalent to 16 degrees in our stimulus display settings, corresponding to roughly twice the average size of an ON and OFF subdomain (~8 deg diameter). For each image sub-region, we detected edges using the Prewitt method (function edge.m, Matlab) and analysed the orientations of the detected edges performing a Hough transformation (using the function Hough.m, Matlab). We defined the local orientation for that image sub-region as that with the highest variance in the Standard Hough Transform matrix of the image. A variance threshold of 3.5 was set to match the visual perception of edges in a subset of images. Image sub-regions were considered ‘‘oriented’’ if the variance exceeded this threshold and ‘‘non-oriented’’ otherwise. Varying the threshold did not change the results (data not shown). In relation to each image sub-region we then calculated the proportion of other image sub-regions with similar orientations (ΔOrientation < 30 degrees) in the collinear axis of the sub-region's orientation and the axis orthogonal to it as a function of distance (**Fig. 12f**).

2.2.10 Statistics

All statistical tests used in the manuscript were non-parametric, with no assumptions concerning normality or equality of variances. Statistical significance of sample distributions of the difference in orientation preference between dendrites and spines were determined with a permutation test (**Figs. 6e,f, 3d,e, 12a,b,c,h,i**). Permutation tests do not assume normality of underlying distributions, nor need the observations be independent. We randomly permuted the preferred orientation of the spines, calculated the difference in orientation preference between dendrites and spines for this shuffled dataset and computed the mean of the distribution. We repeated this procedure 10000 times to obtain a distribution of values, and calculated the fraction of values exceeding the actual value of the non-permuted data. For **Fig. 6c,d**, the randomization procedure involved randomly permuting the RF distance for spine-dendrite pairs and then calculating an F statistic for the shuffled dataset. This procedure was repeated 10000 times in order to assess the percentage of repetitions that produce F values greater than those obtained for the non-permuted data. This percentage then provided an estimate of the P values associated with RF distance effects under the null hypothesis. This procedure preserves the number of data points in each bin, addressing the problem of having few data points for a given group.

For **Fig. 1g** and **Fig. 3d** the inter-spine distance was binned and the mean spatial RF correlation for spine pairs within each bin was calculated independently for each dendrite. The permutation

test was performed by randomly permuting the spatial RF correlations within the different dendrites. Only dendrites with more than 6 spines with significant RFs were included in this analysis. The same analysis was applied for the similarity in orientation preference instead of spatial RF correlation in **Fig. 1h** and **Fig. 3e**. These analyses were performed on the level of dendrites rather than individual spines to provide very conservative statistics, to avoid potential overestimation of significance due to the large number of spine pairs, and because of the combination of dependent and independent data. Pooling all data and performing the permutation test on individual spine pairs gave very similar results. Other statistical tests used are described in the main text or the figure legends. No sample size calculation was performed, but sample sizes are consistent with those generally employed in the field.

2.3. RESULTS

To determine the visual response properties of synaptic inputs onto neurons in mouse primary visual cortex (V1) we used two-photon imaging of calcium signals in dendritic spines (Chen et al., 2013, 2011; Wilson et al., 2016) on L2/3 pyramidal cells sparsely expressing the genetically encoded calcium indicator GCaMP6s (Chen et al., 2013) (**Fig. 1a**). Through this technique, neurons are labelled with a fluorescent protein whose emission intensity is dependent on firing rate. This allows neuronal activity to be read out as variations in basal fluorescence. Using sparse noise stimuli, we mapped the structure of spatial receptive fields (RFs) based on calcium signals observed in individual dendritic spines and nearby dendritic stretches (**Fig. 1b-e**).

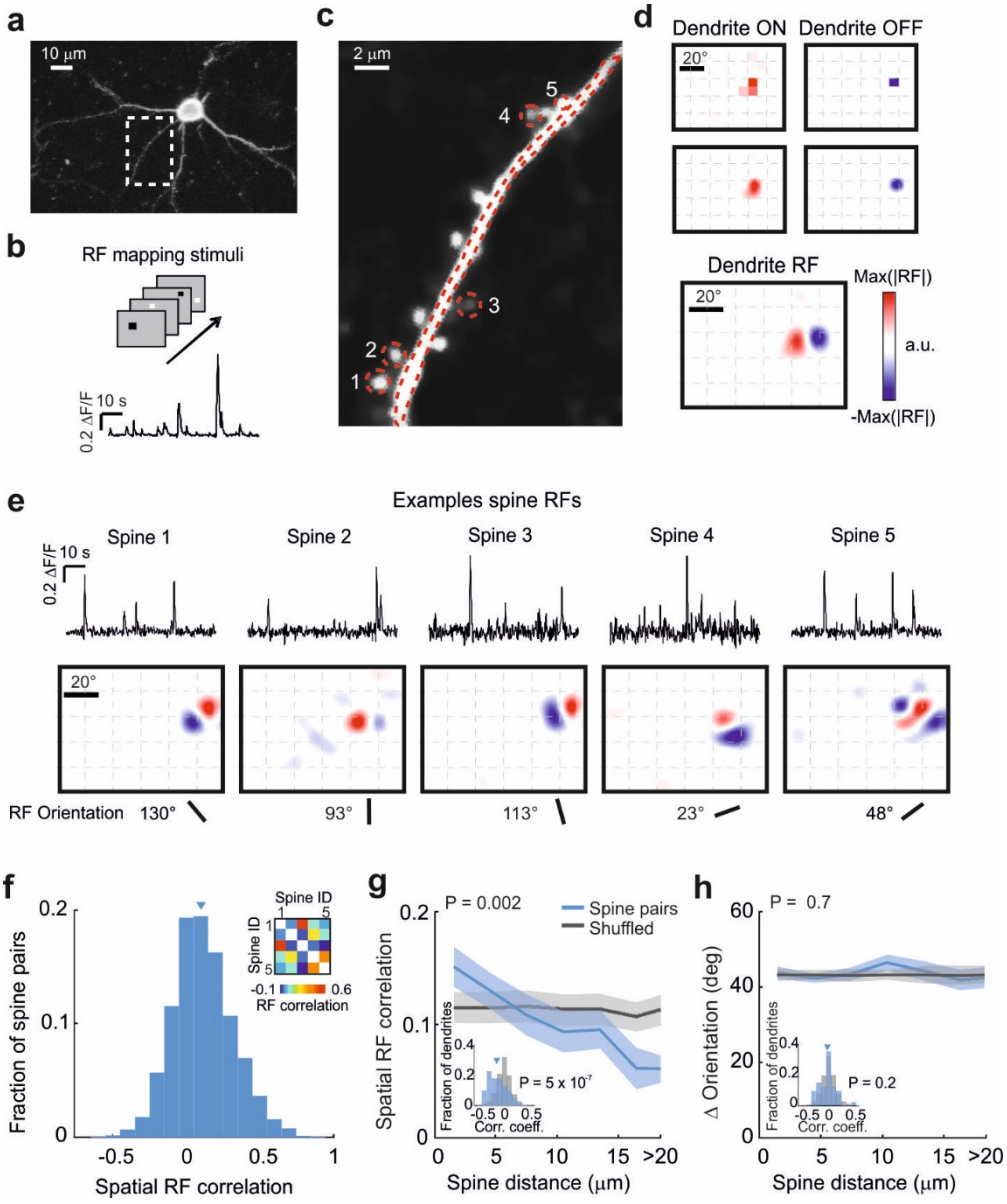

Figure 1 | Dendritic clustering of synaptic inputs with similar receptive fields

a, Z-projection of a layer 2/3 neuron expressing GCaMP6s in mouse V1. **b**,**c** Schematic of receptive field (RF) mapping stimuli and a representative calcium signal (**b**) of the dendritic segment (**c**) indicated in **a**. **d**, Raw (top), smoothed (middle) and combined (bottom) ON and OFF RF subfield maps from calcium signals extracted from the ROI over the dendrite shown in **c**. **e**, Spine calcium signals after removal of the dendritic component (top row), smoothed RFs (middle row), and orientation preference derived from the RFs (bottom row) of the example spines in **c**. **f**, The distribution of pairwise spatial RF correlation coefficients for all imaged spine pairs (N=3966 spine pairs, 74 dendrites, 21 mice). Triangle indicates median. Inset, example matrix of correlation coefficients of RFs from the spines in **c** and **e**. **g,h**, Relationship between the dendritic distance separating pairs of spines and their spatial RF correlation coefficients (**g**) and between spine-pair distances and the difference in their orientation preference (**h,** ΔOrientation). Shadings represent SEM. P-values from permutation test. Inset, the distribution of correlation coefficients between spine pair distance and spatial RF correlation (**g**), or difference in orientation preference (**h)** for individual dendrites. P-values from Wilcoxon signed-rank test, N= 3728 spine pairs, 39 dendrites, 18 mice.

We isolated synaptic responses of individual spines by removing the contribution of the dendritic calcium signal from the spine calcium signal using robust regression (Chen et al., 2013; Wilson et al., 2016) (**Fig. 2;** see Methods). To verify that the results yielded by this method were not biased by potential non-linearities in the integration of spine signals with active dendritic signals, we repeated our analysis on only a subset of data where we could detect isolated spines signals in the absence of dendritic activity (**Fig. 12;** see Methods).

We found that 49% of spines were visually responsive (n = 1017/ 2072 spines, 21 mice), and 69% of those exhibited significant spatial RFs (**Fig. 1e**; RF size = 211 ± 78 degrees^2, mean ± SD). The spatial RF describes the relative position of ON (response to light increments) and OFF (response to light decrements) subfields in visual space, and provides information about visual features to which a neuron is most sensitive, including their orientation, phase, spatial frequency, location and size.

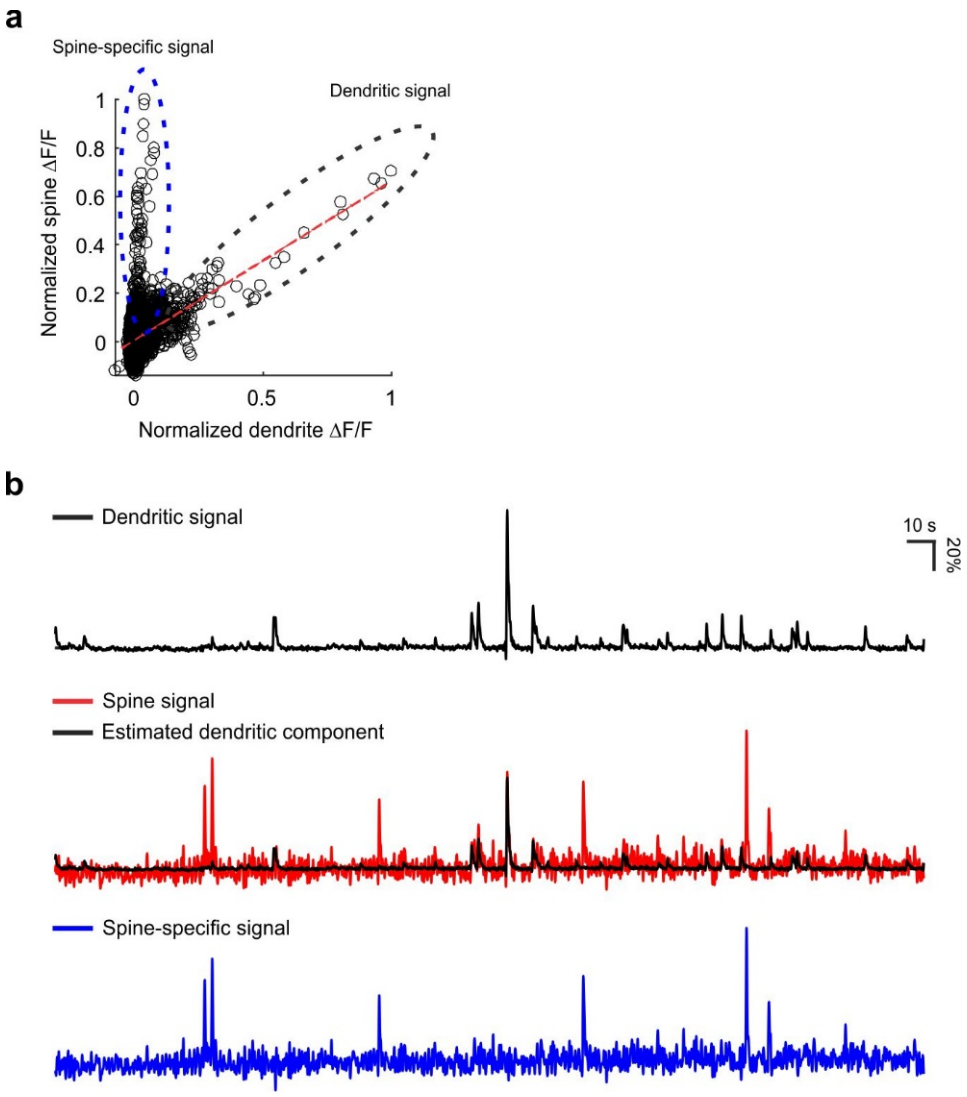

Figure 2 | Isolation of spine-specific signals using robust regression

a, Calcium signal in the spine as a function of the signal in the corresponding dendritic shaft for one example spine. The slope of the robust fit (red dashed line), which indicates the contribution of dendritic activity to the spine signal, was used as a scaling factor. The scaled dendrite signal was then subtracted from the spine signal. **b**, Example traces of the calcium signal in the dendrite (top), the signal in the spine and the estimated dendritic component (scaled dendrite signal, middle) and the isolated spine-specific signal after subtraction (bottom).

2.3.1 Input clustering

We first asked how spines with different visual feature preferences were distributed along the dendrite and if neighbouring spines shared preferences for visual features. As a measure of RF similarity, we computed a pixel-by-pixel correlation coefficient between pairs of RF maps (Cossell et al., 2015). On average, spatial RF correlations were weakly positive (0.1 ± 0.2, mean ± SD), but RF shapes and positions were very diverse, and only a small fraction of inputs shared highly similar RF maps (**Fig. 1f**, 4.4% spine pairs with spatial RF correlation > 0.5). Importantly, nearby spines were more likely to have correlated RF maps than spines further apart (**Fig. 1g**, P = 0.002). Consistent with previous results (Chen et al., 2013), this clustering did not depend on similarity of orientation preference (**Fig. 1h**, P = 0.7), as determined from the apposition angle of ON and OFF subfields of each RF (**Fig. 3**; see Methods), but instead on the co-localisation of RF subfields in visual space (**Fig. 4**). Therefore, synaptic inputs tend to cluster over short dendritic distances if they respond to similar visual features that occupy similar regions in visual space, consistent with observations that neighboring inputs are more frequently co-active (Kleindienst et al., 2011; Takahashi et al., 2012).

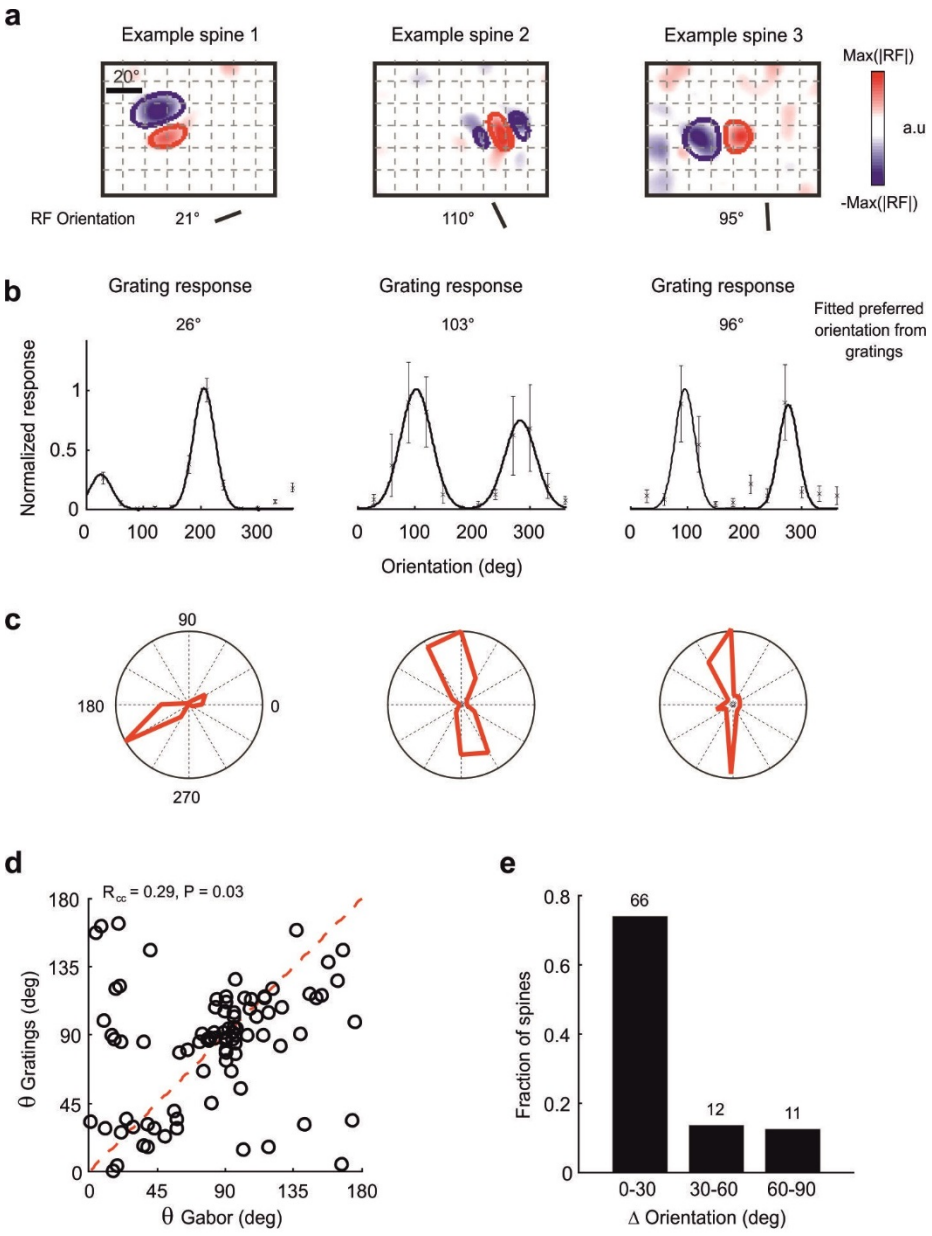

Figure 3 | The relationship between orientation preference derived from spine RFs and drifting grating responses.

a, Smoothed RFs (top), and orientation preference extracted from the RFs (bottom) for three example spines. **b**, Example orientation tuning curves obtained using sinusoidal gratings for the same spines as in **a.** Normalized responses were fitted with the sum of two Gaussians (See Methods). Error bars indicate SEM. **c**, Polar plots of the grating responses above in **b**. **d**, Correspondence of orientation preference derived from responses to drifting gratings and from the RF Gabor fit of individual spines. Correlation coefficient and p-value from circular correlation, n = 89 spines. **e**, The distribution of spines relative to the difference in their orientation

preference derived from RFs and grating responses (ΔOrientation). The majority of spines show similar orientation preferences for the two methods.

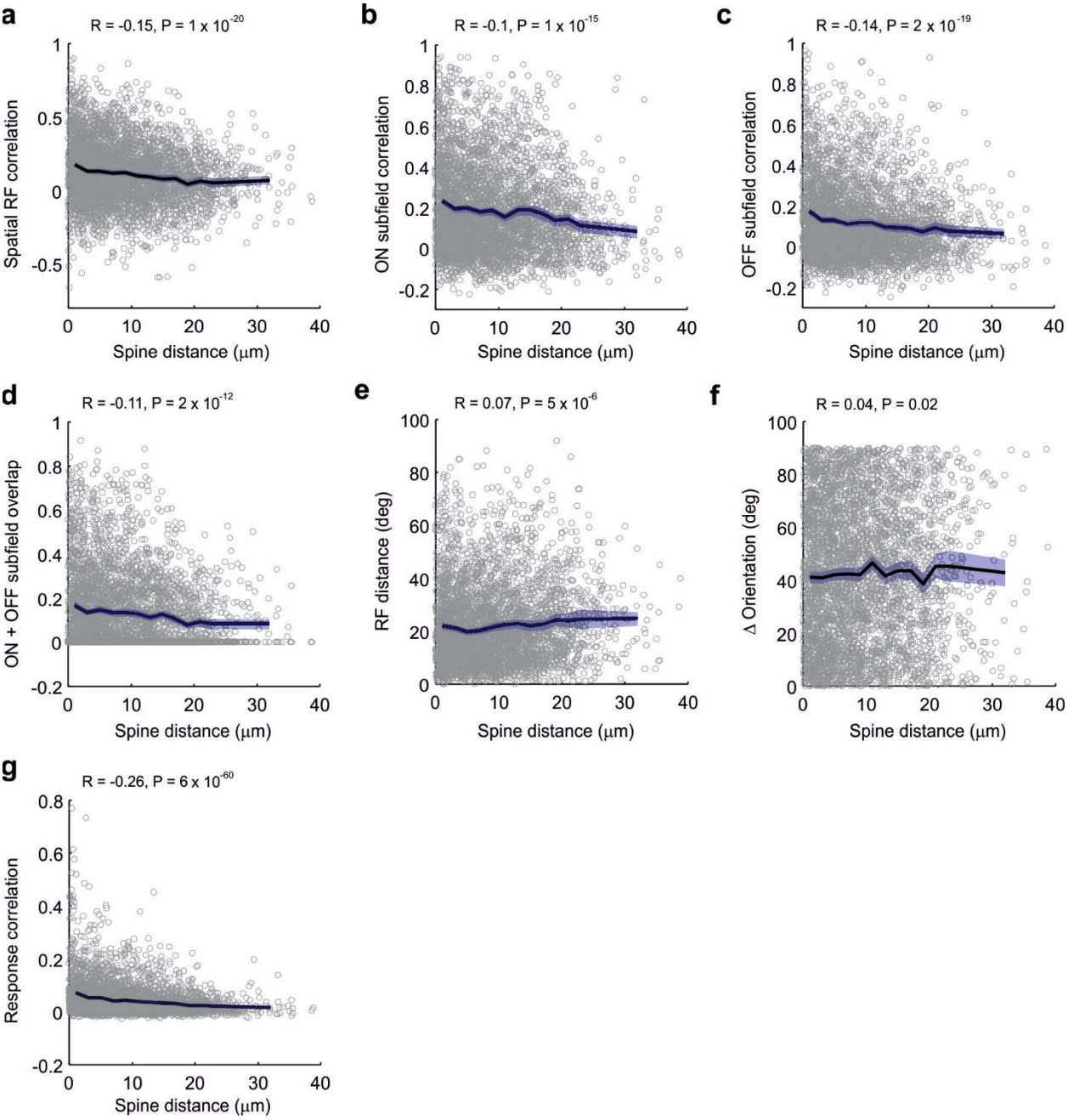

Figure 4 | The relationship between spine pair distance and different visual response properties

a-g, Dendritic separation of spines pairs versus RF similarity (**a**, spatial RF correlation coefficients), ON subfield correlation coefficient (**b**), OFF subfield correlation coefficient (**c**), ON + OFF RF overlap (**d,** see Methods), RF

centre distance (**e**), difference in orientation preference (**f**, ΔOrientation), and correlation coefficient of calcium signals (**g,** total correlation). N = 3966 spine pairs, 74 dendrites, 21 mice. Blue shading represents the 95% confidence interval of the mean.

2.3.2 Relationship between RF properties and connectivity

To compare response properties of synaptic inputs with those of the postsynaptic cell, we also mapped the spatial RFs of dendrites on which the spines resided (**Fig. 1d**, **Fig. 5a**). Dendritic calcium signals extended across entire branches within the imaged region (correlation coefficient between dendritic segments = 0.91 ± 0.08), and RFs derived from dendritic activity closely resembled those derived from calcium signals in the cell body (**Fig. 6**). Under our experimental conditions, most dendritic signals thus likely arose from action potentials back-propagating from the soma or were generated in the dendrite but induced somatic action potentials (Markram et al., 1995; Smith et al., 2013; Stuart and Spruston, 2015; Svoboda et al., 1999). Therefore, we used global dendritic signals as a proxy for the output activity of the postsynaptic neuron.

Computing the distance in visual space between RF centres of the postsynaptic neuron and its spines allowed us to determine the distribution of inputs from different parts of the visual field (**Fig. 5a**). Although the majority of inputs overlapped retinotopically (43% spines, 243/563, spine-dendrite RF centre distance < 15 degrees), the RFs of 28% of spines (159/563) were separated by more than 30 degrees from the neuron's RF and therefore provided visual information from positions outside of the neuron's classical RF (**Fig. 5a,b**). The majority of synaptic inputs with displaced RFs likely originates from neurons > 200 μm apart (**Fig. 7**) or from sources outside of V1. These retinotopically displaced visual inputs were more numerous on more superficial neurons and dendrites, and on higher-order dendrites further away from the cell body (**Fig. 5c,d** and **Fig. 8**).

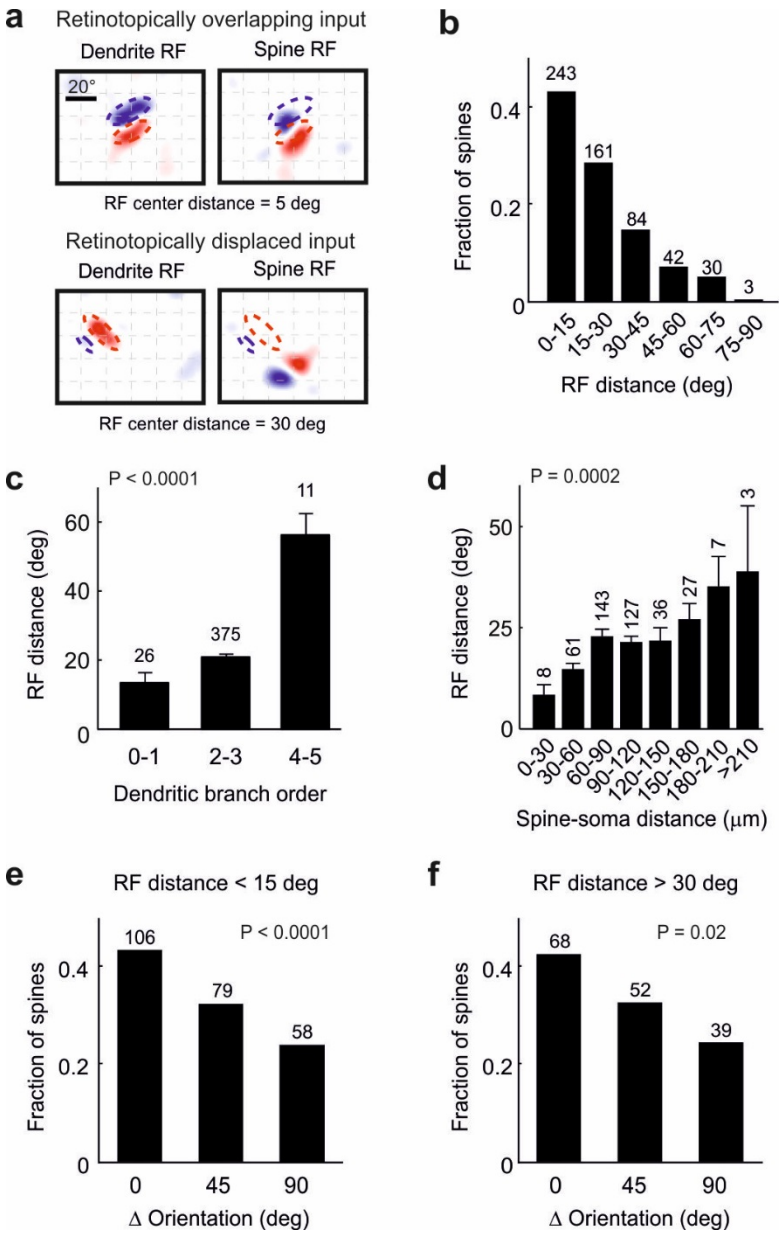

Figure 5 | Organisation of synaptic inputs from extended regions of visual space

a, Example RFs for two spine-dendrite pairs with either overlapping (top) or displaced RFs (bottom). Dashed lines indicate the dendrite RF Gabor fit outline. **b**, Distribution of distances in visual space between the RFs of spines and their corresponding dendrite. (N=62 dendrites, 21 mice). **c**, Mean spine - dendrite RF distance as a function of branch order of the imaged dendritic segment. Error bars represent SEM. **d**, Mean spine - dendrite RF distance as a function of the physical distance between spine and soma along the dendritic tree. **e**-**f**, The frequency of spines as a function of the difference between their preferred orientation (ΔOrientation) and that of the corresponding dendrite, for spine-dendrite pairs with retinotopically overlapping RFs (**e**), and for retinotopically displaced inputs (**f**). The numbers above bars indicate the number of spine - dendrite pairs. P-values are derived from permutation tests (see Methods).

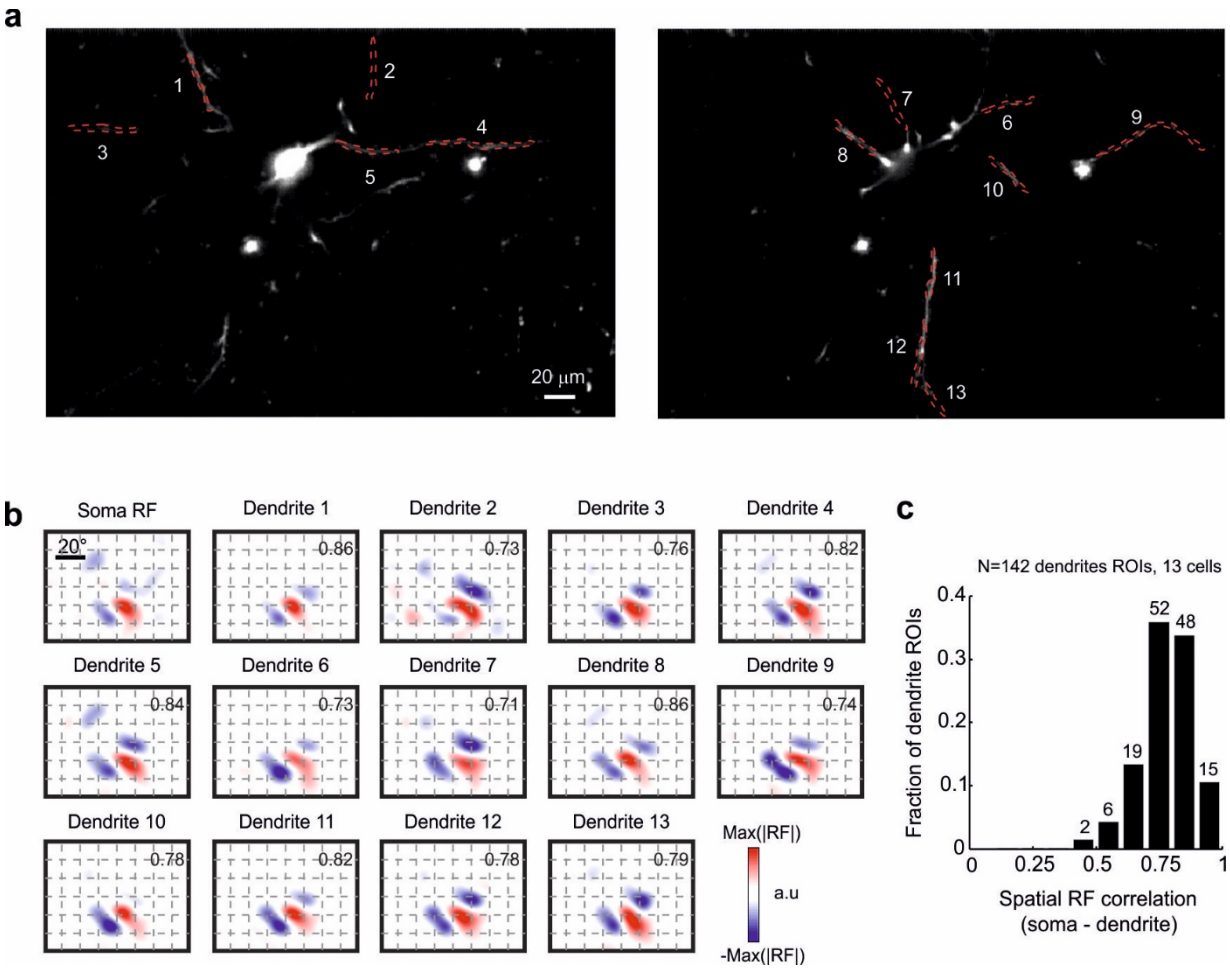

Figure 6 | Simultaneous imaging of dendritic and somatic calcium signals.

a, Two imaging planes separated by 10 □m comprising the soma and dendrites of a V1 layer 2/3 neuron expressing GCaMP6s. Dashed red lines indicate 13 dendritic ROIs from the same neuron. **b,** RFs calculated from calcium signals in the cell body and in the dendritic ROIs indicated in **a.** Numbers in the upper right corner of the dendritic RF maps indicate correlation with the somatic RF map. **c,** The frequency of dendrite ROIs as a function of the similarity of their RF with that of the soma (pixel-by-pixel RF map correlation). The majority of dendrites show similar RFs to that of the soma**.**

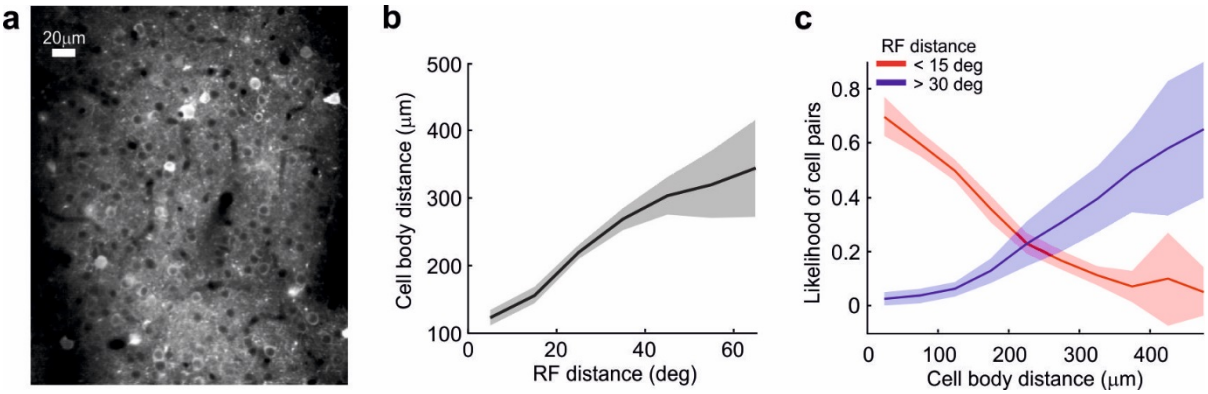

Figure 7 | Relationship between the physical distance of somata and the distance of their RFs

a, Example imaging region with layer 2/3 neurons expressing GCaMP6s. **b**, Median physical cell body distance of all cell pairs as a function of the distance in visual space of their RFs. Shading indicates 95% confidence interval. **c**, Likelihood of encountering cell pairs with overlapping (< 15 deg distance, red) and displaced (> 30 deg distance, blue) RFs for different physical cell body distances.

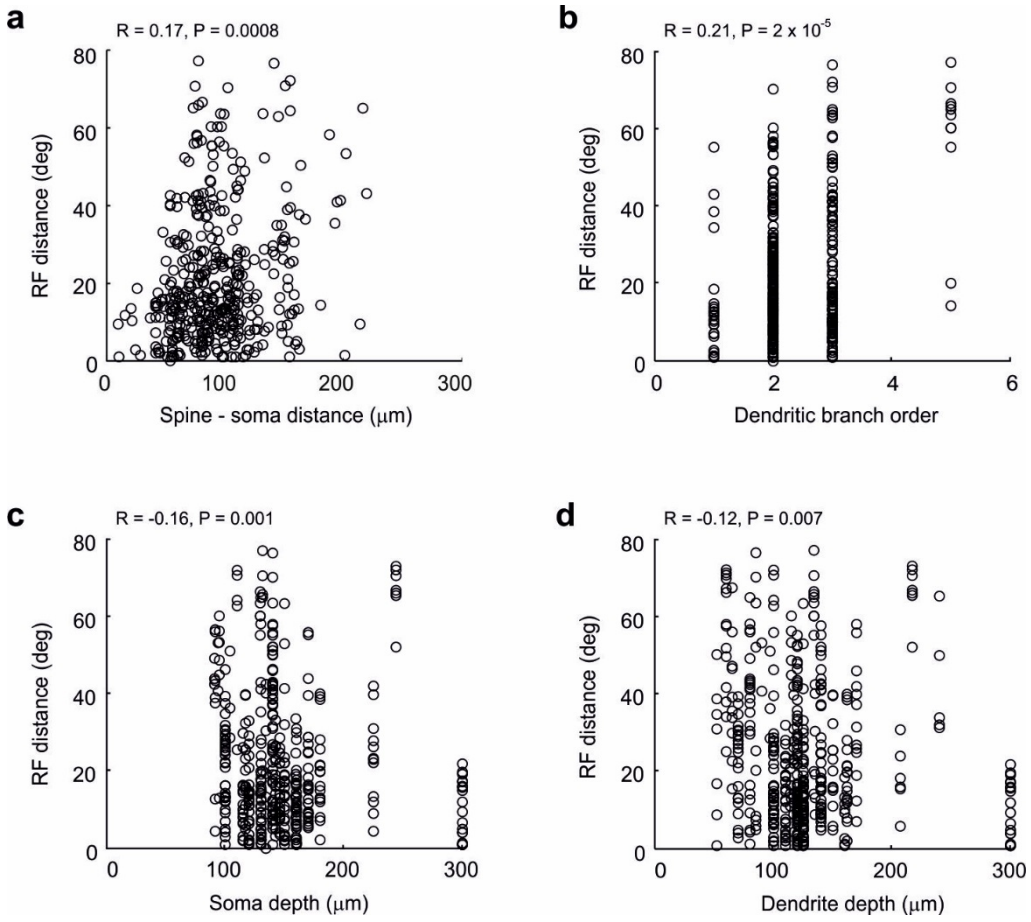

Figure 8 | Anatomical location of spines with retinotopically displaced RFs

a-d, Distance in visual space of the RFs of spines from that of the parent neuron as a function of the physical distance between spine and soma measured along the dendritic tree (**a**), of the dendritic branch order of the dendrite (**b**), of the depth of the soma beneath the cortical surface (**c**), and of the depth of the imaged dendrite (**d**).

We found a coarse retinotopic organization of visual inputs across the dendritic tree with a significant gradient in visual space elevation relative to the postsynaptic cell's RF, consistent with the direction of retinotopic gradients in mouse V1 (**Fig. 10**).

We next determined the relationship between the visual feature preferences of synaptic inputs and the postsynaptic neuron, and examined how this relationship changes as a function of RF separation. Of synaptic inputs whose RFs largely overlapped with that of the postsynaptic neuron (RF centre distance < 15 degrees), many preferred orientations similar to that of the postsynaptic neuron, while fewer inputs preferred orthogonal orientations (**Fig. 5e**, $P < 0.0001$, permutation

test). These results are consistent with previous studies showing functionally specific connectivity in local networks in visual cortex (Cossell et al., 2015; Lee et al., 2016; Wertz et al., 2015a)

In contrast, little is known about the functional properties of synaptic inputs originating from cells that process visual information remote from the RF of the postsynaptic neuron, even though these constitute a substantial fraction of inputs onto cortical neurons (Binzegger et al., 2004; Markov et al., 2011; Stepanyants et al., 2009). We found that synaptic inputs with RFs displaced by more than 30 degrees from the RF of the postsynaptic cell also showed functional specificity, with the majority of inputs preferring orientations similar to the postsynaptic neuron (**Fig. 5f**, P = 0.02).

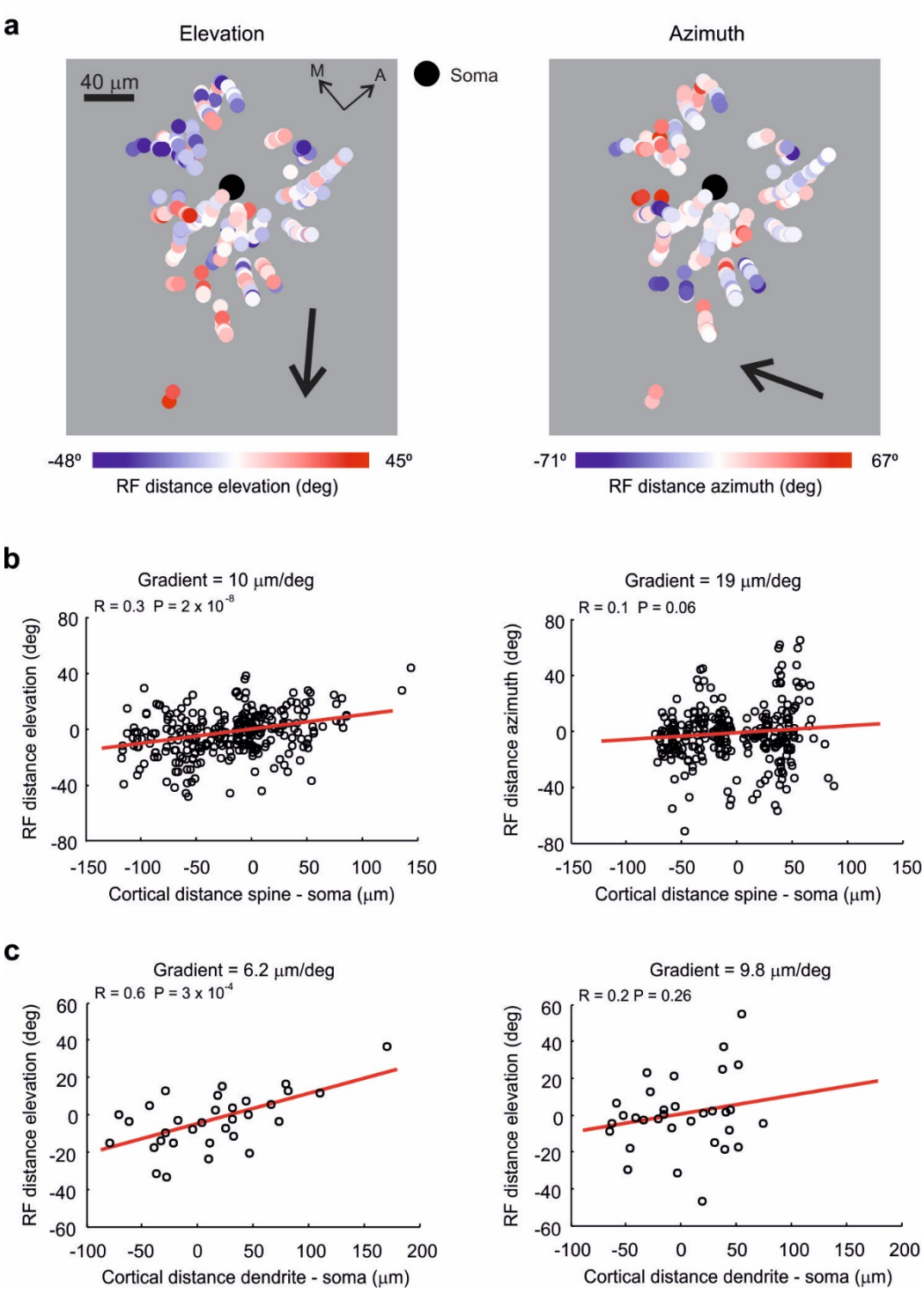

Figure 9 | Retinotopic organization of visual inputs.

a, Position of colored dots indicates the cortical position of spines relative to the cell body on a plane parallel to the cortical surface. Dots are color-coded according to the spines' RF position in visual field elevation (left) and visual field azimuth (right) relative to the parent neuron's RF. Spines from all cells are combined, aligned to the cell body position shown by the black dot. Arrows indicate axes of cortical space that correlate best with

changes in receptive field elevation (left) or azimuth (right). **b,** Relationship between RF distance in elevation (left) and azimuth (right) and cortical distance of spines and soma in the direction of the best fit as indicated by arrows in **a**. **c,** Relationship between RF distance in elevation (left) and azimuth (right) and cortical distance of dendrites and soma in the direction of the best fit as indicated by arrows in **a**, after averaging the position and RF elevation or RF azimuth of all spines on the same dendritic branch. M: medial, A: anterior. N = 32 dendrites, 15 mice (all dendrites for which the cell body position was recovered).

2.3.3 Organisation of visual inputs with displaced RFs

The RF of the recorded cells and their inputs lie in various locations of the visual field and their size and orientation vary. Therefore, to be able to combine all data in single plots, we first rotated and translated the RF of each neuron to match a template RF structure (**Fig 10)**. The same transformation was then applied to the RFs of the presynaptic inputs, which allowed us to pool together all input RFs (**Fig 11b,c**). The organisation of connectivity strongly depended on the position of the input RFs relative to the RF of the postsynaptic cell (**Fig. 11**). Specifically, the relationship between orientation preference and connectivity was only apparent for inputs with RFs displaced in visual space along or close to the axis of the postsynaptic neuron's RF orientation ('co-axial visual space', P = 0.001; **Fig. 11a,b,d**). In contrast, retinotopically displaced inputs from the axis orthogonal to the postsynaptic neuron's RF orientation were less numerous ('orthogonal visual space', 39%, 62/159 visually displaced RFs), and they were not biased towards sharing the postsynaptic neuron's orientation preference, but were as likely to prefer orthogonal orientations (**Fig. 11c,e**, P = 0.7). We further compared other RF parameters that might account for the observed difference. The structure, size and goodness of Gaussian fit of input RFs in co-axial and orthogonal visual space were similar as well as their distribution along the dendritic tree (see Methods, all P-Values > 0.1, Kolmogorov-Smirnov tests). Thus neurons with displaced RFs preferentially connect if their RFs are co-oriented and aligned along the axis of their preferred orientation. This functionally specific connectivity between neurons processing different parts of visual space matches the statistics of edge co-occurrence in natural images, wherein edges of the same orientation occur more often along a common axis (**Fig. 11f**; see Methods) (Geisler et al., 2001; Sigman et al., 2001)

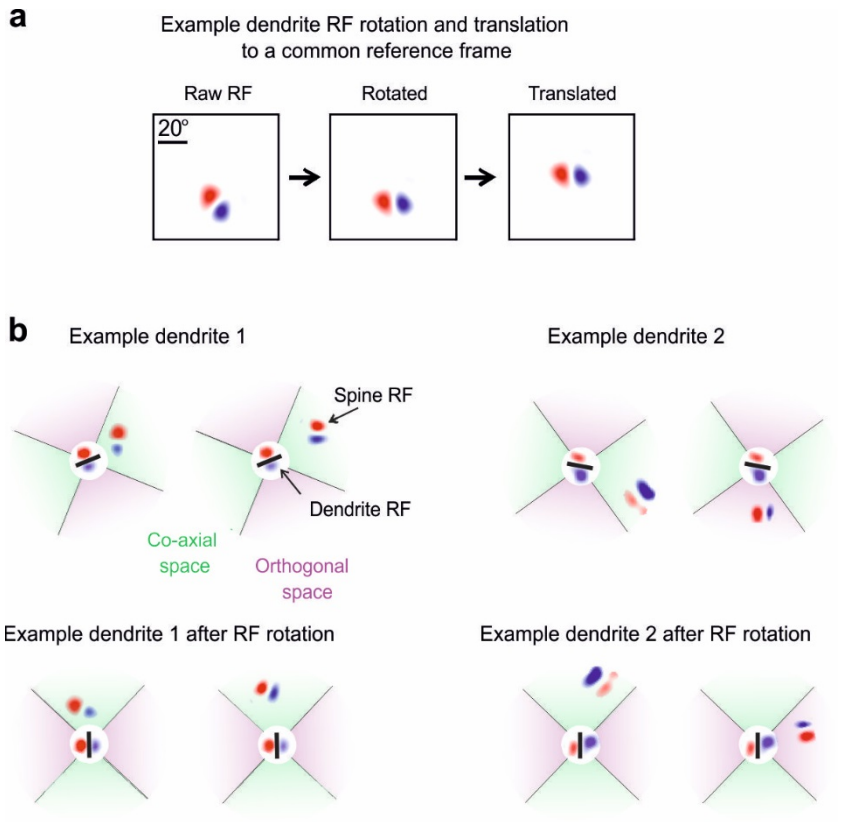

Figure 10 | Transformation of dendrite and spine RFs

Transformation of RFs of dendrites and their corresponding spines for pooling of all spine RFs in **Figure 3b, c**. **a**, To combine the position and orientation of all spine RFs relative to dendritic RFs in a common coordinate framework, we rotated the dendritic RFs such that their orientation was vertical and then translated them such that their centres were aligned at the same position. The parameters of this transformation were then used to transform the RFs of all spines to maintain the spatial relationship of their RF to that of their parent dendrite. **b**, RFs of two example dendrites and two of their corresponding spines before (top) and after transformation (bottom) as described in **a.** The visual space was defined as co-axial (green) or orthogonal (purple) relative to the centre and orientation of the dendrite RF.

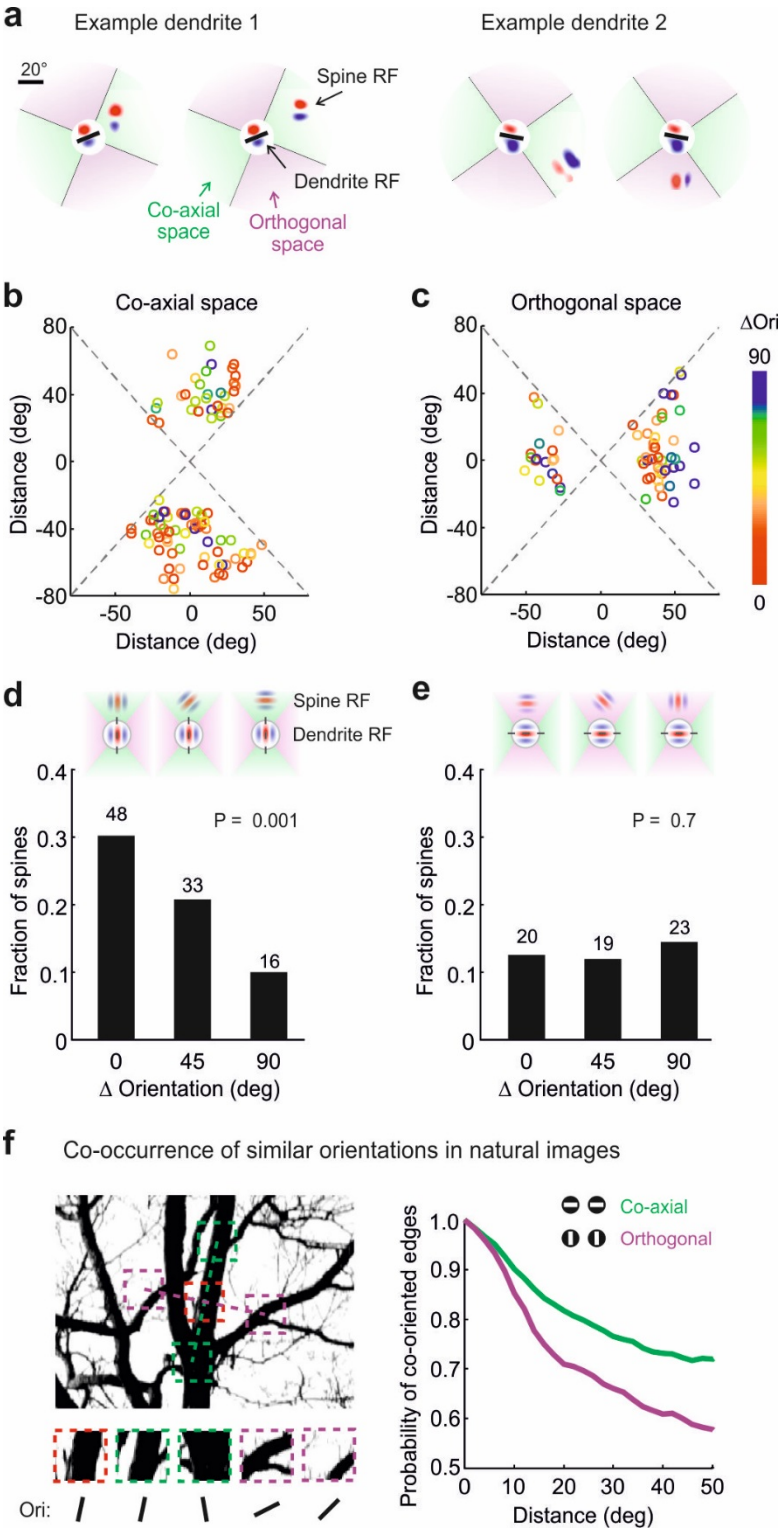

Figure 11 | Preferential synaptic input from neurons with co-oriented and co-axially aligned receptive fields.

a, Two example dendrite RFs with two retinotopically displaced spine RFs each. The visual field was divided into two sectors relative to the orientation of the dendrite RF: the co-axial visual space refers to the region around

the orientation axis of the RF (< ± 45 deg) running through its centre, the orthogonal region occupies the remainder of visual space. **b-c**, Position in visual space and orientation difference relative to the dendrite RF of spines with displaced RFs located in co-axial (**b**, 97 spines) or orthogonal (**c**, 62 spines) visual space. Circles indicate individual spines. Colour denotes the difference in orientation preference (ΔOrientation) between the spine and dendrite. **d-e**, The frequency of spines with displaced RFs as a function of the difference in their preferred orientation from that of the corresponding dendrite for spines with RFs located in co-axial (**d**) or orthogonal (**e**) visual space. Schematics above illustrate the relationship between spine and dendrite RFs for each bin. Spine numbers are indicated above bars. P-values from permutation tests, N = 44 dendrites, 17 mice. **f**, Left: example natural image. Green and purple squares represent co-axially and orthogonally displaced image sub-regions from a reference sub-region (red square). Right: probability of co-occurrence of features with similar orientations (ΔOrientation < 30 deg) in natural images for pairs of image features spatially displaced co-axially or orthogonally according to their orientation. The two distributions are significantly different for all displacements beyond 2 degrees (2 to 50 degrees, bin size 2 degrees, P< 0.01, Wilcoxon rank sum tests, Bonferroni correction for multiple comparisons).

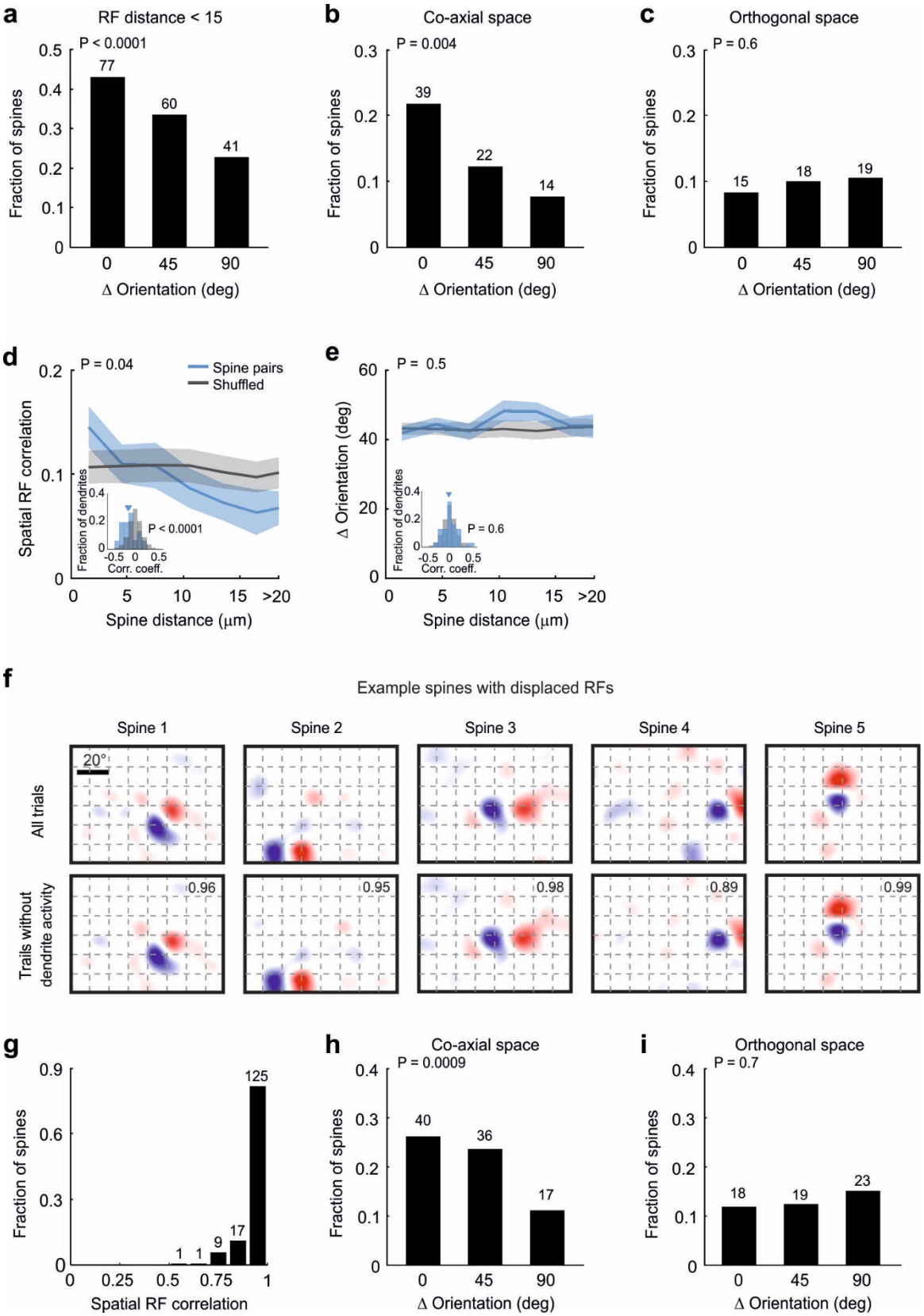
a
RF distance < 15
P < 0.0001
77
60
41
Fraction of spines
Δ Orientation (deg)
b
Co-axial space
P = 0.004
39
22
14
c
Orthogonal space
P = 0.6
15
18
19
d
P = 0.04
Spine pairs
Shuffled
Spatial RF correlation
Fraction of dendrites
P < 0.0001
Corr. coeff.
Spine distance (μm)
e
P = 0.5
Δ Orientation (deg)
P = 0.6
f
Example spines with displaced RFs
Spine 1
Spine 2
Spine 3
Spine 4
Spine 5
All trials
Trails without dendrite activity
20°
0.96
0.95
0.98
0.89
0.99
g
125
17
9
1
1
Spatial RF correlation
h
Co-axial space
P = 0.0009
40
36
17
i
Orthogonal space
P = 0.7
18
19
23

Figure 12 | Control analysis for potential artefacts caused by global dendritic signals

a-e, Main analyses repeated after including only spines with responses not significantly correlated with the activity of their corresponding dendrite (see Methods, N = 522 spines, 26% of spines removed). **a**, corresponds to Figure 2e. **b**, corresponds to Figure 3d. **c**, corresponds to Figure 3e. **d**, corresponds to Figure 1g. **e**, corresponds to Figure 1h. **f-i**, Analyses of displaced spine RFs repeated after excluding all stimulus presentation trials in which the dendrite showed a calcium transient. **f**, Example RFs computed including all trials (top) or only trials in which the dendrite was not active (bottom). Numbers in the upper right corner indicate spatial RF correlation between the two RFs. **g**, Frequency of spines as a function of the similarity of their RF maps (spatial RF correlation) computed with and without trials with dendrite activity. **h**, corresponds to Figure 3d. **i**, corresponds to Figure 3e.

3. Discussion

3.1 Summary

The work presented in this thesis was aimed at exploring for the first time the functional organization of visual excitatory inputs from different areas of the visual field on a single-cell level.

Using two-photon calcium imaging in dendritic spines in L2/3 neurons of the mouse visual cortex, we were able to infer from the activity of single spines the activity of the synaptically connected axonal projections and thus the activity of the presynaptic neurons. This enabled us to determine what information a neuron receives from different locations of visual space. We were further able to compare the visual responses of these inputs to those of the postsynaptic cells in order to investigate the functional similarities between interconnected neurons. Our results confirm that functional connectivity rules exist between neurons representing different areas of the visual field. These rules are comparable with those previously described in local networks, with a further twist, thus expanding the current knowledge of functional connectivity.

This discussion chapter will sequentially address the main findings as well as the relevance of these results along with some challenges in their interpretation.

3.2 Spine signals

Changes in the intracellular calcium concentration are highly correlated with voltage changes inside neurons (Baker et al., 1971; Chen et al., 2013; Sabatini et al., 2002). This allows the visualization of suprathreshold spiking activity in neuronal somata and dendrites (Jia et al., 2010; Ohki et al., 2005; Svoboda et al., 1997), as well as detecting subthreshold synaptic inputs in dendritic spines (Chen et al., 2013, 2011; Jia et al., 2011; Yuste and Denk, 1995), probably due to the fact that they are highly compartmentalized (Yuste et al., 2000; Yuste and Denk, 1995).

In cortical pyramidal cells, excitatory synapses are formed on the dendritic spines. As such, the activity of a single excitatory input is reflected in calcium transients mediated by NMDA receptors (Chen et al., 2011; Mainen et al., 1999), which are largely confined to the spine this input contacts (Chen et al., 2011). Thus, we can use the calcium activity of single spines to infer the activity of the presynaptic cells and to characterize their responses to various visual stimuli.

Dendritic spine imaging offers significant advantages for studying functional connectivity: 1. certainty about the connection between two cells, 2. access to a wide range of inputs from diverse sources; 3. access to information not only regarding the functional properties of the inputs but also their distribution and potential impact on the activity of the postsynaptic cell. The main disadvantage of this technique is that the origin and cell type of the presynaptic neuron remains unknown.

3.3 Clustering

We find that inputs representing similar visual features from overlapping locations in visual space are more likely to terminate on nearby spines. This relationship was governed by the similarity of spatial RFs of neighboring inputs and did not extend to other functional properties such as orientation preference. One might wonder why, as the orientation selectivity of a neuron is believed to be a product of its receptive field structure (Lien and Scanziani, 2013).

There are several reasons why we did not observe clustering of inputs with similar orientation preference. We inferred orientation preference from the RF structure rather than directly from responses to oriented gratings. Therefore, one possibility is that the noise in the estimated preference masks the effect. However, the distribution of orientation preferences of local synaptic inputs we found is very similar to that observed in previous studies that used oriented grating stimuli (Ko et al., 2011; Lee et al., 2016; Wertz et al., 2015a), indicating that orientation preference can be estimated relatively well from the RF structure. This is confirmed by our control experiments in which we directly compared orientation preference inferred from RFs with that extracted from responses to moving gratings in individual spines. Most importantly, a recent study that mapped orientation preference of individual spines using drifting grating stimuli also did not find a relationship between orientation preference and physical distance of individual spines of layer 2/3 neurons in V1 (Chen et al., 2013).

As of yet, there is a lack of consensus regarding spatial clustering of functionally similar inputs in sensory areas. Some studies do find a tendency for this type of organization (Kleindienst et al., 2011; Takahashi et al., 2012; Wilson et al., 2016), while others see a relatively heterogeneous distribution of inputs (Chen et al., 2013, 2011). Notably, a recent study found that co-localization of similarly tuned inputs can be cell-specific and branch-specific and that the proportion of

branches exhibiting a higher proportion of co-tuned inputs correlates with the cells' overall degree of orientation tuning (Wilson et al., 2016). In this study clustering was investigated on a larger spatial scale which leaves open the question of how these results translate to the level of neighboring spines.

Computational work and experimental observations support a functional role for this type of organization in signal integration and input-output computations. Neighboring inputs might cooperate to generate non-linear dendritic events that contribute to a neuron's output (Smith et al., 2013; Stuart and Spruston, 2015; Weber et al., 2016). The correlated activity of neighboring synaptic inputs in response to sensory stimulation might contribute to NMDA current amplification and the generation of dendritic spikes, which provide an orientation-tuned signal to the soma and therefore may play a role in sharpening cortical feature selectivity (Lavzin et al., 2012; Smith et al., 2013).

Despite the preferential connectivity based on feature preference similarity, neurons receive a functionally wide array of inputs, leading to broadly tuned subthreshold potentials (Cossell et al., 2015; Jia et al., 2010). The orientation selectivity of the spiking output of many cells is higher than would be inferred from subthreshold responses combined with a spiking non-linearity. The clustering of functionally related inputs can lead to local dendritic events and increase the probability of action potential generation (Palmer et al., 2014) in response to particular visual features. Therefore, clustering of similar synaptic inputs could produce orientation-tuned dendritic spikes, providing a more selective signal to the soma than would be conveyed by the passive summation of postsynaptic potentials (Smith et al., 2013). This mechanism could therefore increase response selectivity of the neuron's output, explaining the degree of tuning observed on the level of action potential firing (Smith et al., 2013; Wilson et al., 2016).

3.4 Organization of inputs

We have investigated the spatial arrangement of retinotopically displaced inputs relative to the location of visual space they represent. A rough retinotopic organization of inputs is evident in our data. Inputs with displaced RFs tend to form synapses on higher order dendrites, further away from the cell body and are present in greater proportion on more superficial dendrites and cells. Unfortunately, expression of the calcium indicator was too low in distal dendrites to image spine

signals. limiting us to record from dendrites relatively close to the cell body. Therefore, the depth of the soma and that of the imaged dendrites are strongly correlated in our dataset. This prevented us from distinguishing which is the more important factor for the targeting of inputs with displaced RFs, depth of the cell body or the targeted dendrite.

Our results indicate a finer retinotopic organization only in the elevation axis. This could be due to an unequal sampling of the cortical space in the two axes. Post hoc analysis revealed a bias in our dataset, which contains more remote dendrites in the cortical axis representing elevation than that representing azimuth. Regardless, we could show for the first time that in mouse V1 visual space is to some extent mapped on a subcellular level.

3.5 Functional connectivity

To date the relationship between connectivity and in vivo function has been more extensively studied within local cortical networks, mostly due to fewer technical limitations in identifying and simultaneously recording interconnected cells. Several studies using various techniques have generated information about connectivity rules in local networks, all reaching the same conclusion: local connectivity is governed by functional similarity (Cossell et al., 2015; Ko et al., 2011; Lee et al., 2016; Wertz et al., 2015a). Neurons tuned for similar visual features have a higher rate of connectivity and form stronger bilateral connections.

This study aimed to expand the current knowledge on functional connectivity by focusing on inputs with displaced RFs. We determined that the majority of these inputs originate from beyond the local network due to the lack of overlap between their RFs and those of the postsynaptic cells. The degree of separation of the RFs in visual space indicates that these inputs are likely conveyed by long-range projections.

We go beyond anatomical studies which determined the larger scale regional targets of these projections, since we were able to measured input connectivity of individual neurons. We find a bias in the proportion of inputs from functionally similar cells. The postsynaptic neurons receive significantly more connections from cells with similar orientation selectivity. This result is in keeping with previous anatomical studies showing that long range connections preferentially link similar orientation columns (Bosking et al., 1997; Gilbert and Wiesel, 1989; Malach et al., 1993; Martin et al., 2014; Mitchison and Crick, 1982). Our results not only functionally confirm this

connection specificity but furthermore prove that the same wiring strategy persists also in species whose visual cortex lacks columnar organization for orientation selectivity.

In addition to preferential connectivity based on orientation preference similarity, we show that that connectivity of putative long-range inputs is also selective on another level: inputs with displaced RFs do not only share the orientation preference of the postsynaptic cells, but their receptive fields are also aligned along the axis of the preferred orientation. This collinearity of the RFs confirms predictions from anatomical studies performed in different mammalian species which found that long range projections preferentially extend along the axis of the preferred orientation of their origin site (Bosking et al., 1997; Schmidt et al., 1997; Sincich and Blasdel, 2001).

3.6 Functional relevance

This specific pattern of connectivity suggests that the presence of collinearly arranged line segments might enhance the responses of the postsynaptic neurons (Ito and Gilbert, 1999; Kapadia et al., 1995; Polat and Norcia, 1998), thus accounting for surround facilitation effects. This hypothesis is supported by previous studies in cat and primate V1 showing that co-oriented, collinear stimuli have a facilitating effect on neuronal responses (Kapadia et al., 1995; Nelson and Frost, 1985). For example, a neuron's response to a stimulus within its receptive field is enhanced by adding another stimulus in the surround region, provided that both stimuli match the preferred orientation of the RF and are collinearly placed (Kapadia et al., 1995). Additionally, increasing the number of collinear stimuli has a proportional effect on neuronal responses (Li et al., 2008).

Surround facilitation is, however, a far less common effect than surround suppression. Many studies describe surround suppression as predominant and some have in fact failed to detect facilitation (Bolz and Gilbert, 1986; Cavanaugh et al., 2002a, 2002b; Gilbert and Wiesel, 1990; Nelson and Frost, 1978; Self et al., 2014).

The answer to these differences might lie in the configuration of the visual stimuli used to investigate surround effects. Many of these studies use full surround stimuli or stimuli that span both the RF and the surround region. This might be a key feature in the distinction between suppression and facilitation, as facilitation has been shown to tightly depend on the exact position and structure of the stimulus, as mentioned previously, and divergence from the optimal

configuration results in effects of opposite sign (Grinvald et al., 1994; Kapadia et al., 1995; Levitt and Lund, 1997; Sengpiel and Blakemore, 1996). Additionally, different subclasses of cells exhibit various surround interactions at different positions relative to their RFs: end inhibition, side inhibition, uniform inhibition, end facilitation, side facilitation etc.

It has been proposed that a uniform surround suppression is generally present, probably through an interplay of different mechanisms (Adesnik et al., 2012; Bolz and Gilbert, 1986; Self et al., 2014), to which location specific effects are added through facilitation carried by long range lateral connections (Samonds et al., 2017).

Lastly and importantly, the RF structure is not a rigid property, but neuronal responses can vary strongly depending on stimulus configuration or experimental context (David et al., 2004; Sharpee et al., 2006; Yeh et al., 2009). Therefore, surround effects could differ depending on the behavioral context.

The collinear arrangement of long-range projections supports a role in mediating the visual processing of spatially extended contours, as suggested by anatomical and physiological studies (Bosking et al., 1997; Crook et al., 2002; Gilbert and Wiesel, 1989; Kapadia et al., 1995; Malach et al., 1993; Mitchison and Crick, 1982; Nelson and Frost, 1985; Schmidt et al., 1997; Ts'o et al., 1986). A classical contour integration paradigm requires the linking of orientation across space to detect a contour (Field et al., 1993). Distant neurons with orientation-matched, coaxial RFs would be co-activated by contours or edges extending in visual space, and could thus provide the circuit elements promoting facilitation of V1 responses by collinearly arranged line segments (Kapadia et al., 1995; Nelson and Frost, 1985; Polat, 1999).

Psychophysical studies show that the ability to detect a contour depends on the position and orientation of its segments (Field et al., 1993), further supporting collinear facilitation as a mechanism for contour detection. Collinear facilitation and side-inhibition have been proposed to help detect and group orientated contours within complex backgrounds (Kapadia et al., 1995; Li et al., 2006; Polat and Norcia, 1998).

Contour detection belongs to a class of perceptual phenomena governed by the Gestalt rules of "good continuation", which seem to parallel the functional nature of long-range interactions (Field et al., 1993; Geisler et al., 2001; Kovács, 1996; Polat, 1999; Sigman et al., 2001; Yen and Finkel,

1998) and which serve to sort and selectively combine local signals and integrate this information into global object representations.

3.7 Origin of inputs with displaced RFs

The main potential sources of inputs with displaced RFs include lateral projections within V1, feedback from higher visual areas and axonal projections from the thalamus. Two thalamic nuclei project densely to primary visual cortex, the dLGN and the lateral posterior nucleus (LP) (Roth et al., 2015). The RF structures of neurons in both of these regions are quite dissimilar from those of the displaced inputs we have analyzed. LGN RFs are generally smaller and round, while LP RFs are up to six times larger than both LGN or cortical RFs (Durand et al., 2016) and are less structured (Roth et al., 2015). As the structure of thalamic RFs does not resemble those in our dataset, a thalamic origin of these inputs is improbable.

Feedback from higher visual areas has been proposed to participate in some of the surround RF effects (Angelucci and Bressloff, 2006; Gilbert and Li, 2013), but the receptive field properties of many of these areas are also on average not well matched to those of the receptive fields we have recorded: The size of higher visual area RFs is significantly larger than those in V1 (Van den Bergh et al., 2010; Wang and Burkhalter, 2007), and there is a higher proportion of complex RFs (Van den Bergh et al., 2010), which would be excluded from our analysis due to insufficient lack of segregation between the ON and OFF subfields.

Therefore, the most likely source of the inputs with displaced RFs we recorded are horizontal connections within V1, from neurons at different positions in the V1 retinotopic map, in agreement with the previously described anatomical characteristics of horizontal, long-range projections in other mammalian species.

3.8 Development of specific cortical connectivity

How does this specific connectivity arise? Previous studies have revealed that precise feedforward connectivity is established first, is responsible for the functional identity and is largely maintained during development (Chapman and Stryker, 1993; Espinosa and Stryker, 2012; Ko et al., 2013).

Preferential recurrent connectivity, however, seems much more sensitive to rearrangement and refinement during periods of increased plasticity as it is not mature at eye opening and instead develops gradually in the first weeks of visual experience (Ko et al., 2013). Very likely, activity-dependent mechanisms of plasticity come into play, preserving and strengthening inputs that lead to correlated firing while pruning or weakening connections between uncorrelated cells.

In the local network, neurons with similar RFs respond to roughly the same location of the visual field and will be co-activated by the same stimuli, probably leading to the strengthening of their connections. For neurons whose RFs lie in different parts of visual space, the statistics of natural scenes support the specific connectivity we observe. Elongated edges spanning large areas of the visual field are enriched in the environment (Geisler et al., 2001; Sigman et al., 2001), such that the collinearity of interconnected but spatially displaced RFs leads to increased co-activation of neurons whose RFs fall along the same edge, potentially resulting in the strengthening of connections between them.

Anatomical evidence from studies in cats indicates that an experience-dependent process is involved in the refinement of long range connections, which are uniformly distributed in the first postnatal week and start increasing their precise targeting of iso-orientation columns over the following period (Callaway and Katz, 1990).

3.9 Outlook

Future experiments would aim to confirm previous physiological and psychophysical results in carnivores and primates by testing the existence of collinear facilitation in awake behaving mice. A previous study has shown that functionally specific connectivity in local networks develops even in the absence of visual experience (Ko et al., 2013). We hypothesize that long-range connectivity is highly dependent on visual experience, specifically on the structure of visual input. If this is true, visual deprivation would be expected to have a drastic effect on the preferential selection and strengthening of long-range inputs, abolishing the relationship between functional similarity and connectivity. Furthermore, such a paradigm might allow to test whether functionally specific long-range connectivity is indeed required for collinear facilitation and/or contour detection.

The organization and functional properties of synaptic inputs which provide behavior-related top-down modulation, as well as how these non-sensory signals are integrated with visual input is

another potential subject of future investigation. The ultimate goal would be to follow the function and structure of individual spines while animals are trained in visually-guided learning tasks in order to detect learning-related changes in different synaptic inputs and how these relate to changes in the function of the associated neuron.

4. References

Adesnik, H., Bruns, W., Taniguchi, H., Huang, Z.J., Scanziani, M., 2012. A neural circuit for spatial summation in visual cortex. Nature 490, 226–231. doi:10.1038/nature11526

Alitto, H.J., Usrey, W.M., 2015. Surround suppression and temporal processing of visual signals. J. Neurophysiol. 113, 2605. doi:10.1152/jn.00480.2014

Alitto, H.J., Usrey, W.M., 2008. Origin and Dynamics of Extraclassical Suppression in the Lateral Geniculate Nucleus of the Macaque Monkey. Neuron 57, 135–146. doi:10.1016/j.neuron.2007.11.019

Alonso, J.-M., Usrey, W.M., Reid, R.C., 2001. Rules of Connectivity between Geniculate Cells and Simple Cells in Cat Primary Visual Cortex. J. Neurosci. 21, 4002.

Angelucci, A., Bressloff, P.C., 2006. Contribution of feedforward, lateral and feedback connections to the classical receptive field center and extra-classical receptive field surround of primate V1 neurons, in: Martinez-Conde, S., Macknik, S.L., Martinez, L.M., Alonso, J.-M., Tse, P.U. (Eds.), Visual Perception, Progress in Brain Research. Elsevier, pp. 93–120. doi:10.1016/S0079-6123(06)54005-1

Angelucci, A., Levitt, J.B., Walton, E.J.S., Hupé, J.-M., Bullier, J., Lund, J.S., 2002. Circuits for Local and Global Signal Integration in Primary Visual Cortex. J. Neurosci. 22, 8633.

Atallah, B.V., Bruns, W., Carandini, M., Scanziani, M., 2012. Parvalbumin-Expressing Interneurons Linearly Transform Cortical Responses to Visual Stimuli. Neuron 73, 159–170. doi:10.1016/j.neuron.2011.12.013

Baden, T., Berens, P., Franke, K., Rosón, M.R., Bethge, M., Euler, T., 2016. The functional diversity of retinal ganglion cells in the mouse. Nature 529, 345–350. doi:10.1038/nature16468

Baker, P.F., Hodgkin, A.L., Ridgway, E.B., 1971. Depolarization and calcium entry in squid giant axons. J. Physiol. 218, 709–755. doi:10.1113/jphysiol.1971.sp009641

Barlow, H.B., Hill, R.M., 1963. Selective Sensitivity to Direction of Movement in Ganglion Cells of the Rabbit Retina. Science 139, 412. doi:10.1126/science.139.3553.412

Bartfeld, E., Grinvald, A., 1992. Relationships between orientation-preference pinwheels, cytochrome oxidase blobs, and ocular-dominance columns in primate striate cortex. Proc. Natl. Acad. Sci. U. S. A. 89, 11905–11909.

Baylor, D.A., Lamb, T.D., Yau, K.W., 1979. Responses of retinal rods to single photons. J. Physiol. 288, 613–634.

Behrens, C., Schubert, T., Haverkamp, S., Euler, T., Berens, P., 2016. Connectivity map of bipolar cells and photoreceptors in the mouse retina. eLife 5, e20041. doi:10.7554/eLife.20041

Beierlein, M., Gibson, J.R., Connors, B.W., 2003. Two Dynamically Distinct Inhibitory Networks in Layer 4 of the Neocortex. J. Neurophysiol. 90, 2987. doi:10.1152/jn.00283.2003

Bi, G., Poo, M., 1998. Synaptic Modifications in Cultured Hippocampal Neurons: Dependence on Spike Timing, Synaptic Strength, and Postsynaptic Cell Type. J. Neurosci. 18, 10464.

Binzegger, T., Douglas, R.J., Martin, K.A.C., 2004. A Quantitative Map of the Circuit of Cat Primary Visual Cortex. J. Neurosci. 24, 8441. doi:10.1523/JNEUROSCI.1400-04.2004

Bock, D.D., Lee, W.-C.A., Kerlin, A.M., Andermann, M.L., Hood, G., Wetzel, A.W., Yurgenson, S., Soucy, E.R., Kim, H.S., Reid, R.C., 2011. Network anatomy and in vivo physiology of visual cortical neurons. Nature 471, 177–182. doi:10.1038/nature09802

Bolz, J., Gilbert, C.D., 1989. The Role of Horizontal Connections in Generating Long Receptive Fields in the Cat Visual Cortex. Eur. J. Neurosci. 1, 263–268. doi:10.1111/j.1460-9568.1989.tb00794.x

Bolz, J., Gilbert, C.D., 1986. Generation of end-inhibition in the visual cortex via interlaminar connections. Nature 320, 362–365. doi:10.1038/320362a0

Bonhoeffer, T., Grinvald, A., 1991. Iso-orientation domains in cat visual cortex are arranged in pinwheel-like patterns. Nature 353, 429–431. doi:10.1038/353429a0

Bonin, V., Mante, V., Carandini, M., 2005. The Suppressive Field of Neurons in Lateral Geniculate Nucleus. J. Neurosci. 25, 10844. doi:10.1523/JNEUROSCI.3562-05.2005

Bosking, W.H., Zhang, Y., Schofield, B., Fitzpatrick, D., 1997. Orientation Selectivity and the Arrangement of Horizontal Connections in Tree Shrew Striate Cortex. J. Neurosci. 17, 2112.

Bowmaker, J.K., Dartnall, H.J., 1980. Visual pigments of rods and cones in a human retina. J. Physiol. 298, 501–511.

Bowmaker, J.K., Dartnall, H.J., Lythgoe, J.N., Mollon, J.D., 1978. The visual pigments of rods and cones in the rhesus monkey, Macaca mulatta. J. Physiol. 274, 329–348. doi:10.1113/jphysiol.1978.sp012151

Boycott, B., Wässle, H., 1999. Parallel processing in the mammalian retina: the Proctor Lecture. Invest. Ophthalmol. Vis. Sci. 40, 1313–1327.

Boycott, B.B., Wässle, H., 1991. Morphological Classification of Bipolar Cells of the Primate Retina. Eur. J. Neurosci. 3, 1069–1088. doi:10.1111/j.1460-9568.1991.tb00043.x

Brainard, D.H., 1997. The Psychophysics Toolbox. Spat. Vis. 10, 433–436. doi:https://doi.org/10.1163/156856897X00357

Branco, T., Clark, B.A., Häusser, M., 2010. Dendritic Discrimination of Temporal Input Sequences in Cortical Neurons. Science 329, 1671. doi:10.1126/science.1189664

Branco, T., Häusser, M., 2011. Synaptic Integration Gradients in Single Cortical Pyramidal Cell Dendrites. Neuron 69, 885–892. doi:10.1016/j.neuron.2011.02.006

Briggs, F., Usrey, W.M., 2008. Emerging views of corticothalamic function. Sens. Syst. 18, 403–407. doi:10.1016/j.conb.2008.09.002

Callaway, E., Katz, L., 1990. Emergence and refinement of clustered horizontal connections in cat striate cortex. J. Neurosci. 10, 1134.

Cannon, M.W., Fullenkamp, S.C., 1991. Spatial interactions in apparent contrast: Inhibitory effects among grating patterns of different spatial frequencies, spatial positions and orientations. Vision Res. 31, 1985–1998. doi:10.1016/0042-6989(91)90193-9

Cavanaugh, J.R., Bair, W., Movshon, J.A., 2002a. Selectivity and Spatial Distribution of Signals From the Receptive Field Surround in Macaque V1 Neurons. J. Neurophysiol. 88, 2547. doi:10.1152/jn.00693.2001

Cavanaugh, J.R., Bair, W., Movshon, J.A., 2002b. Nature and Interaction of Signals From the Receptive Field Center and Surround in Macaque V1 Neurons. J. Neurophysiol. 88, 2530. doi:10.1152/jn.00692.2001

Chapman, B., Stryker, M., 1993. Development of orientation selectivity in ferret visual cortex and effects of deprivation. J. Neurosci. 13, 5251.

Chen, C., Regehr, W.G., 2000. Developmental Remodeling of the Retinogeniculate Synapse. Neuron 28, 955–966. doi:10.1016/S0896-6273(00)00166-5

Chen, T.-W., Wardill, T.J., Sun, Y., Pulver, S.R., Renninger, S.L., Baohan, A., Schreiter, E.R., Kerr, R.A., Orger, M.B., Jayaraman, V., Looger, L.L., Svoboda, K., Kim, D.S., 2013. Ultrasensitive fluorescent proteins for imaging neuronal activity. Nature 499, 295–300. doi:10.1038/nature12354

Chen, X., Leischner, U., Rochefort, N.L., Nelken, I., Konnerth, A., 2011. Functional mapping of single spines in cortical neurons in vivo. Nature 475, 501–505. doi:10.1038/nature10193

Cheong, S.K., Tailby, C., Solomon, S.G., Martin, P.R., 2013. Cortical-Like Receptive Fields in the Lateral Geniculate Nucleus of Marmoset Monkeys. J. Neurosci. 33, 6864. doi:10.1523/JNEUROSCI.5208-12.2013

Chisum, H.J., Fitzpatrick, D., 2004. The contribution of vertical and horizontal connections to the receptive field center and surround in V1. Vis. Brain 17, 681–693. doi:10.1016/j.neunet.2004.05.002

Chklovskii, D.B., Koulakov, A.A., 2004. MAPS IN THE BRAIN: What Can We Learn from Them? Annu. Rev. Neurosci. 27, 369–392. doi:10.1146/annurev.neuro.27.070203.144226

Chung, S., Ferster, D., 1998. Strength and Orientation Tuning of the Thalamic Input to Simple Cells Revealed by Electrically Evoked Cortical Suppression. Neuron 20, 1177–1189. doi:10.1016/S0896-6273(00)80498-5

Clay Reid, R., Alonso, J.-M., 1995. Specificity of monosynaptic connections from thalamus to visual cortex. Nature 378, 281–284. doi:10.1038/378281a0

Cossell, L., Iacaruso, M.F., Muir, D.R., Houlton, R., Sader, E.N., Ko, H., Hofer, S.B., Mrsic-Flogel, T.D., 2015. Functional organization of excitatory synaptic strength in primary visual cortex. Nature 518, 399–403. doi:10.1038/nature14182

Crook, J.M., Engelmann, R., Löwel, S., 2002. GABA-inactivation attenuates colinear facilitation in cat primary visual cortex. Exp. Brain Res. 143, 295–302. doi:10.1007/s00221-002-1007-y

Crossland, W.J., Uchwat, C.J., 1979. Topographic projections of the retina and optic tectum upon the ventral lateral geniculate nucleus in the chick. J. Comp. Neurol. 185, 87–106. doi:10.1002/cne.901850106

Cruz-Martin, A., El-Danaf, R.N., Osakada, F., Sriram, B., Dhande, O.S., Nguyen, P.L., Callaway, E.M., Ghosh, A., Huberman, A.D., 2014. A dedicated circuit links direction-selective retinal ganglion cells to the primary visual cortex. Nature 507, 358–361.

David, S.V., Vinje, W.E., Gallant, J.L., 2004. Natural Stimulus Statistics Alter the Receptive Field Structure of V1 Neurons. J. Neurosci. 24, 6991. doi:10.1523/JNEUROSCI.1422-04.2004

de Monasterio, F.M., 1978. Properties of ganglion cells with atypical receptive-field organization in retina of macaques. J. Neurophysiol. 41, 1435.

Debanne, D., Gähwiler, B.H., Thompson, S.M., 1997. Bidirectional Associative Plasticity of Unitary CA3-CA1 EPSPs in the Rat Hippocampus In Vitro. J. Neurophysiol. 77, 2851.

Debanne, D., Gähwiler, B.H., Thompson, S.M., 1994. Asynchronous pre- and postsynaptic activity induces associative long-term depression in area CA1 of the rat hippocampus in vitro. Proc. Natl. Acad. Sci. U. S. A. 91, 1148–1152.

Dhande, O.S., Stafford, B.K., Lim, J.-H.A., Huberman, A.D., 2015. Contributions of Retinal Ganglion Cells to Subcortical Visual Processing and Behaviors. Annu. Rev. Vis. Sci. 1, 291–328. doi:10.1146/annurev-vision-082114-035502

Dräger, U.C., 1975. Receptive fields of single cells and topography in mouse visual cortex. J. Comp. Neurol. 160, 269–289. doi:10.1002/cne.901600302

Durand, S., Iyer, R., Mizuseki, K., de Vries, S., Mihalas, S., Reid, R.C., 2016. A Comparison of Visual Response Properties in the Lateral Geniculate Nucleus and Primary Visual Cortex of Awake and Anesthetized Mice. J. Neurosci. 36, 12144. doi:10.1523/JNEUROSCI.1741-16.2016

E Reese, B., Cowey, A., 1987. The crossed projection from the temporal retina to the dorsal geniculate nucleus in rat. doi:10.1016/0306-4522(87)90255-7

Ebrey, T., Koutalos, Y., 2001. Vertebrate Photoreceptors. Prog. Retin. Eye Res. 20, 49–94. doi:10.1016/S1350-9462(00)00014-8

Espinosa, J.S., Stryker, M.P., 2012. Development and Plasticity of the Primary Visual Cortex. Neuron 75, 230–249. doi:10.1016/j.neuron.2012.06.009

Euler, T., Haverkamp, S., Schubert, T., Baden, T., 2014. Retinal bipolar cells: elementary building blocks of vision. Nat Rev Neurosci 15, 507–519.

Eysel, U.T., Wolfhard, U., 1983. Morphological fine tuning of retinotopy within the cat lateral geniculate nucleus. Neurosci. Lett. 39, 15–20. doi:10.1016/0304-3940(83)90158-1

Famiglietti, E., Kolb, H., 1976. Structural basis for ON-and OFF-center responses in retinal ganglion cells. Science 194, 193. doi:10.1126/science.959847

Feldman, D.E., 2012. The Spike-Timing Dependence of Plasticity. Neuron 75, 556–571. doi:10.1016/j.neuron.2012.08.001

Ferster, D., 1992. Chapter 20 The synaptic inputs to simple cells of the cat visual cortex, in: Mize, R.R., Marc, R.E., Sillito, A.M. (Eds.), Progress in Brain Research. Elsevier, pp. 423–441. doi:10.1016/S0079-6123(08)63625-0

Field, D.J., Hayes, A., Hess, R.F., 1993. Contour integration by the human visual system: Evidence for a local "association field." Vision Res. 33, 173–193. doi:10.1016/0042-6989(93)90156-Q

Fisher, T.G., Alitto, H.J., Usrey, W.M., 2017. Retinal and Nonretinal Contributions to Extraclassical Surround Suppression in the Lateral Geniculate Nucleus. J. Neurosci. 37, 226. doi:10.1523/JNEUROSCI.1577-16.2016

Froemke, R.C., Poo, M., Dan, Y., 2005. Spike-timing-dependent synaptic plasticity depends on dendritic location. Nature 434, 221–225. doi:10.1038/nature03366

Fu, Y., Tucciarone, J.M., Espinosa, J.S., Sheng, N., Darcy, D.P., Nicoll, R.A., Huang, Z.J., Stryker, M.P., 2014. A Cortical Circuit for Gain Control by Behavioral State. Cell 156, 1139–1152. doi:10.1016/j.cell.2014.01.050

Geisler, W.S., Perry, J.S., Super, B.J., Gallogly, D.P., 2001. Edge co-occurrence in natural images predicts contour grouping performance. Vision Res. 41, 711–724. doi:10.1016/S0042-6989(00)00277-7

Ghodrati, M., Khaligh-Razavi, S.-M., Lehky, S.R., 2017. Towards building a more complex view of the lateral geniculate nucleus: Recent advances in understanding its role. Prog. Neurobiol. 156, 214–255. doi:https://doi.org/10.1016/j.pneurobio.2017.06.002

Gilbert, C., Wiesel, T., 1989. Columnar specificity of intrinsic horizontal and corticocortical connections in cat visual cortex. J. Neurosci. 9, 2432.

Gilbert, C., Wiesel, T., 1983. Clustered intrinsic connections in cat visual cortex. J. Neurosci. 3, 1116.

Gilbert, C.D., Li, W., 2013. Top-down influences on visual processing. Nat Rev Neurosci 14, 350–363.

Gilbert, C.D., Wiesel, T.N., 1990. The influence of contextual stimuli on the orientation selectivity of cells in primary visual cortex of the cat. Opt. Physiol. Vis. 30, 1689–1701. doi:10.1016/0042-6989(90)90153-C

Golding, N.L., Spruston, N., 1998. Dendritic Sodium Spikes Are Variable Triggers of Axonal Action Potentials in Hippocampal CA1 Pyramidal Neurons. Neuron 21, 1189–1200. doi:10.1016/S0896-6273(00)80635-2

Golding, N.L., Staff, N.P., Spruston, N., 2002. Dendritic spikes as a mechanism for cooperative long-term potentiation. Nature 418, 326–331. doi:10.1038/nature00854

Gordon, U., Polsky, A., Schiller, J., 2006. Plasticity Compartments in Basal Dendrites of Neocortical Pyramidal Neurons. J. Neurosci. 26, 12717. doi:10.1523/JNEUROSCI.3502-06.2006

Grinvald, A., Lieke, E., Frostig, R., Hildesheim, R., 1994. Cortical point-spread function and long-range lateral interactions revealed by real-time optical imaging of macaque monkey primary visual cortex. J. Neurosci. 14, 2545.

Grubb, M.S., Thompson, I.D., 2003. Quantitative Characterization of Visual Response Properties in the Mouse Dorsal Lateral Geniculate Nucleus. J. Neurophysiol. 90, 3594. doi:10.1152/jn.00699.2003

Guido, W., Lu, S.M., Sherman, S.M., 1992. Relative contributions of burst and tonic responses to the receptive field properties of lateral geniculate neurons in the cat. J. Neurophysiol. 68, 2199.

Guizar-Sicairos, M., Thurman, S.T., Fienup, J.R., 2008. Efficient subpixel image registration algorithms. Opt. Lett. 33, 156–158.

Harris, K.D., Mrsic-Flogel, T.D., 2013. Cortical connectivity and sensory coding. Nature 503, 51–58.

Hartline, H.K., 1938. The discharge of impulses in the optic nerve of Pecten in response to illumination of the eye. J. Cell. Comp. Physiol. 11, 465–478. doi:10.1002/jcp.1030110311

Hebb, D.O., 1949. The organization of behaviour. New York: Wiley.

Helmchen, F., Svoboda, K., Denk, W., Tank, D.W., 1999. In vivo dendritic calcium dynamics in deep-layer cortical pyramidal neurons 2, 989.

Hess, R., Field, D., 1999. Integration of contours: new insights. Trends Cogn. Sci. 3, 480–486. doi:10.1016/S1364-6613(99)01410-2

Hirsch, J.A., Alonso, J.-M., Reid, R.C., 1995. Visually evoked calcium action potentials in cat striate cortex. Nature 378, 612–616. doi:10.1038/378612a0

Hofer, S.B., Ko, H., Pichler, B., Vogelstein, J., Ros, H., Zeng, H., Lein, E., Lesica, N.A., Mrsic-Flogel, T.D., 2011. Differential connectivity and response dynamics of excitatory and inhibitory neurons in visual cortex 14, 1045.

Holtmaat, A., Bonhoeffer, T., Chow, D.K., Chuckowree, J., De Paola, V., Hofer, S.B., Hubener, M., Keck, T., Knott, G., Lee, W.-C.A., Mostany, R., Mrsic-Flogel, T.D., Nedivi, E., Portera-Cailliau, C., Svoboda, K., Trachtenberg, J.T., Wilbrecht, L., 2009. Long-term, high-resolution imaging in the mouse neocortex through a chronic cranial window. Nat Protoc. 4, 1128–1144. doi:10.1038/nprot.2009.89

Howarth, M., Walmsley, L., Brown, T.M., 2014. Binocular Integration in the Mouse Lateral Geniculate Nuclei. Curr. Biol. 24, 1241–1247. doi:10.1016/j.cub.2014.04.014

Hu, B., Li, X., Zhou, Y., Shou, T., 2000. Effects of bicuculline on direction-sensitive relay cells in the dorsal lateral geniculate nucleus (LGNd) of cats. Brain Res. 885, 87–93. doi:10.1016/S0006-8993(00)02946-2

Hubel, D.H., 1960. Single unit activity in lateral geniculate body and optic tract of unrestrained cats. J. Physiol. 150, 91–104. doi:10.1113/jphysiol.1960.sp006375

Hubel, D.H., Wiesel, T.N., 1968. Receptive fields and functional architecture of monkey striate cortex. J. Physiol. 195, 215–243. doi:10.1113/jphysiol.1968.sp008455

Hubel, D.H., Wiesel, T.N., 1962. Receptive fields, binocular interaction and functional architecture in the cat's visual cortex. J. Physiol. 160, 106–154. doi:10.1113/jphysiol.1962.sp006837

Hubel, D.H., Wiesel, T.N., 1959. Receptive fields of single neurones in the cat's striate cortex. J. Physiol. 148, 574–591. doi:10.1113/jphysiol.1959.sp006308

Huberman, A.D., Niell, C.M., 2011. What can mice tell us about how vision works? Trends Neurosci. 34, 464–473. doi:10.1016/j.tins.2011.07.002

Humphrey, A.L., Norton, T.T., 1980. Topographic organization of the orientation column system in the striate cortex of the tree shrew (Tupaia glis). I. Microelectrode recording. J. Comp. Neurol. 192, 531–547. doi:10.1002/cne.901920311

Ito, M., Gilbert, C.D., 1999. Attention Modulates Contextual Influences in the Primary Visual Cortex of Alert Monkeys. Neuron 22, 593–604. doi:10.1016/S0896-6273(00)80713-8

Jabaudon, D., 2017. Fate and freedom in developing neocortical circuits 8, 16042.

Jagadeesh, B., Gray, C., Ferster, D., 1992. Visually evoked oscillations of membrane potential in cells of cat visual cortex. Science 257, 552. doi:10.1126/science.1636094

JAUBERT-MIAZZA, L., GREEN, E., LO, F.-S., BUI, K., MILLS, J., GUIDO, W., 2005. Structural and functional composition of the developing retinogeniculate pathway in the mouse. Vis. Neurosci. 22, 661–676. doi:10.1017/S0952523805225154

Jia, H., Rochefort, N.L., Chen, X., Konnerth, A., 2011. In vivo two-photon imaging of sensory-evoked dendritic calcium signals in cortical neurons. Nat Protoc. 6, 28–35. doi:10.1038/nprot.2010.169

Jia, H., Rochefort, N.L., Chen, X., Konnerth, A., 2010. Dendritic organization of sensory input to cortical neurons in vivo. Nature 464, 1307–1312. doi:10.1038/nature08947

Jia, H., Varga, Z., Sakmann, B., Konnerth, A., 2014. Linear integration of spine Ca(2+) signals in layer 4 cortical neurons in vivo. Proc. Natl. Acad. Sci. U. S. A. 111, 9277–9282. doi:10.1073/pnas.1408525111

Kampa, B.M., Letzkus, J.J., Stuart, G.J., 2007. Dendritic mechanisms controlling spike-timing-dependent synaptic plasticity. Trends Neurosci. 30, 456–463. doi:10.1016/j.tins.2007.06.010

Kapadia, M.K., Ito, M., Gilbert, C.D., Westheimer, G., 1995. Improvement in visual sensitivity by changes in local context: Parallel studies in human observers and in V1 of alert monkeys. Neuron 15, 843–856. doi:10.1016/0896-6273(95)90175-2

Kapadia, M.K., Westheimer, G., Gilbert, C.D., 2000. Spatial Distribution of Contextual Interactions in Primary Visual Cortex and in Visual Perception. J. Neurophysiol. 84, 2048.

Keck, T., Keller, G.B., Jacobsen, R.I., Eysel, U.T., Bonhoeffer, T., Hübener, M., 2013. Synaptic Scaling and Homeostatic Plasticity in the Mouse Visual Cortex In Vivo. Neuron 80, 327–334. doi:10.1016/j.neuron.2013.08.018

Keck, T., Toyoizumi, T., Chen, L., Doiron, B., Feldman, D.E., Fox, K., Gerstner, W., Haydon, P.G., Hübener, M., Lee, H.-K., Lisman, J.E., Rose, T., Sengpiel, F., Stellwagen, D., Stryker, M.P., Turrigiano, G.G., van Rossum, M.C., 2017. Integrating Hebbian and homeostatic plasticity: the current state of the field and future research directions. Philos. Trans. R. Soc. B Biol. Sci. 372. doi:10.1098/rstb.2016.0158

Kepecs, A., Fishell, G., 2014. Interneuron cell types are fit to function. Nature 505, 318–326.

Kerlin, A.M., Andermann, M.L., Berezovskii, V.K., Reid, R.C., 2010. Broadly Tuned Response Properties of Diverse Inhibitory Neuron Subtypes in Mouse Visual Cortex. Neuron 67, 858–871. doi:10.1016/j.neuron.2010.08.002

Kleindienst, T., Winnubst, J., Roth-Alpermann, C., Bonhoeffer, T., Lohmann, C., 2011. Activity-Dependent Clustering of Functional Synaptic Inputs on Developing Hippocampal Dendrites. Neuron 72, 1012–1024. doi:10.1016/j.neuron.2011.10.015

Ko, H., Cossell, L., Baragli, C., Antolik, J., Clopath, C., Hofer, S.B., Mrsic-Flogel, T.D., 2013. The emergence of functional microcircuits in visual cortex. Nature 496, 96–100. doi:10.1038/nature12015

Ko, H., Hofer, S.B., Pichler, B., Buchanan, K.A., Sjöström, P.J., Mrsic-Flogel, T.D., 2011. Functional specificity of local synaptic connections in neocortical networks. Nature 473, 87–91. doi:10.1038/nature09880

Kovács, I., 1996. Gestalten of today: early processing of visual contours and surfaces. Behav. Brain Res. 82, 1–11. doi:10.1016/S0166-4328(97)81103-5

Kuffler, S.W., 1953. DISCHARGE PATTERNS AND FUNCTIONAL ORGANIZATION OF MAMMALIAN RETINA. J. Neurophysiol. 16, 37.

Larkum, M.E., Kaiser, K.M.M., Sakmann, B., 1999. Calcium electrogenesis in distal apical dendrites of layer 5 pyramidal cells at a critical frequency of back-propagating action potentials. Proc. Natl. Acad. Sci. U. S. A. 96, 14600–14604.

Larkum, M.E., Zhu, J.J., Sakmann, B., 1999. A new cellular mechanism for coupling inputs arriving at different cortical layers. Nature 398, 338–341. doi:10.1038/18686

Lavzin, M., Rapoport, S., Polsky, A., Garion, L., Schiller, J., 2012. Nonlinear dendritic processing determines angular tuning of barrel cortex neurons in vivo. Nature 490, 397–401. doi:10.1038/nature11451

Lee, S.-H., Kwan, A.C., Zhang, S., Phoumthipphavong, V., Flannery, J.G., Masmanidis, S.C., Taniguchi, H., Huang, Z.J., Zhang, F., Boyden, E.S., Deisseroth, K., Dan, Y., 2012.

Activation of specific interneurons improves V1 feature selectivity and visual perception. Nature 488, 379–383. doi:10.1038/nature11312

Lee, W.-C.A., Bonin, V., Reed, M., Graham, B.J., Hood, G., Glattfelder, K., Reid, R.C., 2016. Anatomy and function of an excitatory network in the visual cortex. Nature 532, 370–374. doi:10.1038/nature17192

Leinweber, M., Zmarz, P., Buchmann, P., Argast, P., Hübener, M., Bonhoeffer, T., Keller, G.B., 2014. Two-photon Calcium Imaging in Mice Navigating a Virtual Reality Environment. J. Vis. Exp. JoVE 50885. doi:10.3791/50885

Levitt, J.B., Lund, J.S., 1997. Contrast dependence of contextual effects in primate visual cortex. Nature 387, 73–76. doi:10.1038/387073a0

Levy, W.B., Steward, O., 1983. Temporal contiguity requirements for long-term associative potentiation/depression in the hippocampus. Neuroscience 8, 791–797. doi:10.1016/0306-4522(83)90010-6

Li, W., Piëch, V., Gilbert, C.D., 2008. Learning to Link Visual Contours. Neuron 57, 442–451. doi:10.1016/j.neuron.2007.12.011

Li, W., Piëch, V., Gilbert, C.D., 2006. Contour Saliency in Primary Visual Cortex. Neuron 50, 951–962. doi:10.1016/j.neuron.2006.04.035

Li, Y., Lu, H., Cheng, P., Ge, S., Xu, H., Shi, S.-H., Dan, Y., 2012. Clonally related visual cortical neurons show similar stimulus feature selectivity. Nature 486, 118–121. doi:10.1038/nature11110

Lien, A.D., Scanziani, M., 2013. Tuned thalamic excitation is amplified by visual cortical circuits 16, 1315.

Lisman, J., 1989. A mechanism for the Hebb and the anti-Hebb processes underlying learning and memory. Proc. Natl. Acad. Sci. U. S. A. 86, 9574–9578.

Loffler, G., 2008. Perception of contours and shapes: Low and intermediate stage mechanisms. Vis. Res. Rev. 48, 2106–2127. doi:10.1016/j.visres.2008.03.006

Longordo, F., To, M.-S., Ikeda, K., Stuart, G.J., 2013. Sublinear integration underlies binocular processing in primary visual cortex 16, 714.

Lowel, S., Singer, W., 1992. Selection of intrinsic horizontal connections in the visual cortex by correlated neuronal activity. Science 255, 209. doi:10.1126/science.1372754

Lüscher, C., Malenka, R.C., 2012. NMDA Receptor-Dependent Long-Term Potentiation and Long-Term Depression (LTP/LTD). Cold Spring Harb. Perspect. Biol. 4.

Ma, W., Liu, B., Li, Y., Josh Huang, Z., Zhang, L.I., Tao, H.W., 2010. Visual Representations by Cortical Somatostatin Inhibitory Neurons—Selective But with Weak and Delayed Responses. J. Neurosci. 30, 14371. doi:10.1523/JNEUROSCI.3248-10.2010

Magee, J.C., Johnston, D., 1997. A Synaptically Controlled, Associative Signal for Hebbian Plasticity in Hippocampal Neurons. Science 275, 209. doi:10.1126/science.275.5297.209

Mainen, Z.F., Malinow, R., Svoboda, K., 1999. Synaptic calcium transients in single spines indicate that NMDA receptors are not saturated. Nature 399, 151–155. doi:10.1038/20187

Malach, R., Amir, Y., Harel, M., Grinvald, A., 1993. Relationship between intrinsic connections and functional architecture revealed by optical imaging and in vivo targeted biocytin injections in primate striate cortex. Proc. Natl. Acad. Sci. U. S. A. 90, 10469–10473.

Maldonado, P.E., Gödecke, I., Gray, C.M., Bonhoeffer, T., 1997. Orientation Selectivity in Pinwheel Centers in Cat Striate Cortex. Science 276, 1551. doi:10.1126/science.276.5318.1551

Malinow, R., Malenka, R.C., 2002. AMPA Receptor Trafficking and Synaptic Plasticity. Annu. Rev. Neurosci. 25, 103–126. doi:10.1146/annurev.neuro.25.112701.142758

Markov, N.T., Misery, P., Falchier, A., Lamy, C., Vezoli, J., Quilodran, R., Gariel, M.A., Giroud, P., Ercsey-Ravasz, M., Pilaz, L.J., Huissoud, C., Barone, P., Dehay, C.,

Toroczkai, Z., Van Essen, D.C., Kennedy, H., Knoblauch, K., 2011. Weight Consistency Specifies Regularities of Macaque Cortical Networks. Cereb. Cortex 21, 1254–1272. doi:10.1093/cercor/bhq201

Markram, H., Helm, P.J., Sakmann, B., 1995. Dendritic calcium transients evoked by single back-propagating action potentials in rat neocortical pyramidal neurons. J. Physiol. 485, 1–20. doi:10.1113/jphysiol.1995.sp020708

Markram, H., Lübke, J., Frotscher, M., Sakmann, B., 1997. Regulation of Synaptic Efficacy by Coincidence of Postsynaptic APs and EPSPs. Science 275, 213. doi:10.1126/science.275.5297.213

Markram, H., Toledo-Rodriguez, M., Wang, Y., Gupta, A., Silberberg, G., Wu, C., 2004. Interneurons of the neocortical inhibitory system. Nat Rev Neurosci 5, 793–807. doi:10.1038/nrn1519

Martin, K.A.C., Roth, S., Rusch, E.S., 2014. Superficial layer pyramidal cells communicate heterogeneously between multiple functional domains of cat primary visual cortex 5, 5252.

Migliore, M., Shepherd, G.M., 2002. Emerging rules for the distributions of active dendritic conductances. Nat Rev Neurosci 3, 362–370. doi:10.1038/nrn810

Mitchison, G., Crick, F., 1982. Long axons within the striate cortex: their distribution, orientation, and patterns of connection. Proc. Natl. Acad. Sci. U. S. A. 79, 3661–3665.

Morgenstern, N.A., Bourg, J., Petreanu, L., 2016. Multilaminar networks of cortical neurons integrate common inputs from sensory thalamus 19, 1034.

Morin, L.P., Studholme, K.M., 2014. Retinofugal Projections in the Mouse. J. Comp. Neurol. 522, 3733–3753. doi:10.1002/cne.23635

Mountcastle, V.B., 1957. MODALITY AND TOPOGRAPHIC PROPERTIES OF SINGLE NEURONS OF CAT'S SOMATIC SENSORY CORTEX. J. Neurophysiol. 20, 408.

Nelson, J.I., Frost, B.J., 1985. Intracortical facilitation among co-oriented, co-axially aligned simple cells in cat striate cortex. Exp. Brain Res. 61, 54–61. doi:10.1007/BF00235620

Nelson, J.I., Frost, B.J., 1978. Orientation-selective inhibition from beyond the classic visual receptive field. Brain Res. 139, 359–365. doi:10.1016/0006-8993(78)90937-X

Niell, C.M., 2013. Vision: More Than Expected in the Early Visual System. Curr. Biol. 23, R681–R684. doi:10.1016/j.cub.2013.07.049

Niell, C.M., Stryker, M.P., 2008. Highly Selective Receptive Fields in Mouse Visual Cortex. J. Neurosci. 28, 7520. doi:10.1523/JNEUROSCI.0623-08.2008

Nienborg, H., Hasenstaub, A., Nauhaus, I., Taniguchi, H., Huang, Z.J., Callaway, E.M., 2013. Contrast Dependence and Differential Contributions from Somatostatin- and Parvalbumin-Expressing Neurons to Spatial Integration in Mouse V1. J. Neurosci. 33, 11145. doi:10.1523/JNEUROSCI.5320-12.2013

Ohki, K., Chung, S., Ch'ng, Y.H., Kara, P., Reid, R.C., 2005. Functional imaging with cellular resolution reveals precise micro-architecture in visual cortex. Nature 433, 597–603. doi:10.1038/nature03274

Ohtsuki, G., Nishiyama, M., Yoshida, T., Murakami, T., Histed, M., Lois, C., Ohki, K., 2012. Similarity of Visual Selectivity among Clonally Related Neurons in Visual Cortex. Neuron 75, 65–72. doi:10.1016/j.neuron.2012.05.023

Ozeki, H., Finn, I.M., Schaffer, E.S., Miller, K.D., Ferster, D., 2009. Inhibitory Stabilization of the Cortical Network Underlies Visual Surround Suppression. Neuron 62, 578–592. doi:10.1016/j.neuron.2009.03.028

Palmer, L.M., Shai, A.S., Reeve, J.E., Anderson, H.L., Paulsen, O., Larkum, M.E., 2014. NMDA spikes enhance action potential generation during sensory input 17, 383.

Petros, T.J., Rebsam, A., Mason, C.A., 2008. Retinal Axon Growth at the Optic Chiasm: To Cross or Not to Cross. Annu. Rev. Neurosci. 31, 295–315. doi:10.1146/annurev.neuro.31.060407.125609

Pfeffer, C.K., Xue, M., He, M., Huang, Z.J., Scanziani, M., 2013. Inhibition of inhibition in visual cortex: the logic of connections between molecularly distinct interneurons 16, 1068.

Pi, H.-J., Hangya, B., Kvitsiani, D., Sanders, J.I., Huang, Z.J., Kepecs, A., 2013. Cortical interneurons that specialize in disinhibitory control. Nature 503, 521–524.

Piscopo, D.M., El-Danaf, R.N., Huberman, A.D., Niell, C.M., 2013. Diverse Visual Features Encoded in Mouse Lateral Geniculate Nucleus. J. Neurosci. 33, 4642. doi:10.1523/JNEUROSCI.5187-12.2013

Polat, U., 1999. Functional architecture of long-range perceptual interactions. Spat. Vis. 12, 143–162. doi:https://doi.org/10.1163/156856899X00094

Polat, U., Norcia, A.M., 1998. Elongated physiological summation pools in the human visual cortex1Preliminary results were reported at the 1996 Annual Meeting of the Society for Neuroscience: [50].1. Vision Res. 38, 3735–3741. doi:10.1016/S0042-6989(97)00426-4

Polat, U., Sagi, D., 1993. Lateral interactions between spatial channels: Suppression and facilitation revealed by lateral masking experiments. Vision Res. 33, 993–999. doi:10.1016/0042-6989(93)90081-7

Pologruto, T.A., Sabatini, B.L., Svoboda, K., 2003. ScanImage: Flexible software for operating laser scanning microscopes. Biomed. Eng. OnLine 2, 13. doi:10.1186/1475-925X-2-13

Pouille, F., Marin-Burgin, A., Adesnik, H., Atallah, B.V., Scanziani, M., 2009. Input normalization by global feedforward inhibition expands cortical dynamic range 12, 1577.

Priebe, N.J., Ferster, D., 2012. Mechanisms of Neuronal Computation in Mammalian Visual Cortex. Neuron 75, 194–208. doi:10.1016/j.neuron.2012.06.011

Rathbun, D.L., Warland, D.K., Usrey, W.M., 2010. Spike Timing and Information Transmission at Retinogeniculate Synapses. J. Neurosci. 30, 13558. doi:10.1523/JNEUROSCI.0909-10.2010

Reid, R.C., Alonso, J.-M., 1996. The processing and encoding of information in the visual cortex. Curr. Opin. Neurobiol. 6, 475–480. doi:10.1016/S0959-4388(96)80052-3

Renart, A., Song, P., Wang, X.-J., 2003. Robust Spatial Working Memory through Homeostatic Synaptic Scaling in Heterogeneous Cortical Networks. Neuron 38, 473–485. doi:10.1016/S0896-6273(03)00255-1

Rockland, K., Lund, J., 1982. Widespread periodic intrinsic connections in the tree shrew visual cortex. Science 215, 1532. doi:10.1126/science.7063863

Rockland, K.S., Lund, J.S., 1983. Intrinsic laminar lattice connections in primate visual cortex. J. Comp. Neurol. 216, 303–318. doi:10.1002/cne.902160307

Rodieck, R.W., 1967. Receptive Fields in the Cat Retina: A New Type. Science 157, 90. doi:10.1126/science.157.3784.90

Röhlich, P., van Veen, T., Szél, Á., 1994. Two different visual pigments in one retinal cone cell. Neuron 13, 1159–1166. doi:10.1016/0896-6273(94)90053-1

Rompani, S.B., Müllner, F.E., Wanner, A., Zhang, C., Roth, C.N., Yonehara, K., Roska, B., 2017. Different Modes of Visual Integration in the Lateral Geniculate Nucleus Revealed by Single-Cell-Initiated Transsynaptic Tracing. Neuron 93, 767–776.e6. doi:https://doi.org/10.1016/j.neuron.2017.01.028

Roska, B., Werblin, F., 2001. Vertical interactions across ten parallel, stacked representations in the mammalian retina. Nature 410, 583–587. doi:10.1038/35069068

Roth, M.M., Dahmen, J.C., Muir, D.R., Imhof, F., Martini, F.J., Hofer, S.B., 2015. Thalamic nuclei convey diverse contextual information to layer 1 of visual cortex 19, 299.

Runyan, C.A., Schummers, J., Van Wart, A., Kuhlman, S.J., Wilson, N.R., Huang, Z.J., Sur, M., 2010. Response Features of Parvalbumin-Expressing Interneurons Suggest Precise Roles for Subtypes of Inhibition in Visual Cortex. Neuron 67, 847–857. doi:10.1016/j.neuron.2010.08.006

Sabatini, B.L., Oertner, T.G., Svoboda, K., 2002. The Life Cycle of Ca2+ Ions in Dendritic Spines. Neuron 33, 439–452. doi:10.1016/S0896-6273(02)00573-1

Samonds, J.M., Feese, B.D., Lee, T.S., Kuhlman, S., 2017. Non-uniform surround suppression of visual responses in mouse V1. J. Neurophysiol. doi:10.1152/jn.00172.2017

Schiller, J., Major, G., Koester, H.J., Schiller, Y., 2000. NMDA spikes in basal dendrites of cortical pyramidal neurons. Nature 404, 285–289. doi:10.1038/35005094

Schiller, J., Schiller, Y., Stuart, G., Sakmann, B., 1997. Calcium action potentials restricted to distal apical dendrites of rat neocortical pyramidal neurons. J. Physiol. 505, 605–616. doi:10.1111/j.1469-7793.1997.605ba.x

Schmidt, K.E., Goebel, R., Löwel, S., Singer, W., 1997. The Perceptual Grouping Criterion of Colinearity is Reflected by Anisotropies of Connections in the Primary Visual Cortex. Eur. J. Neurosci. 9, 1083–1089. doi:10.1111/j.1460-9568.1997.tb01459.x

Scholl, B., Tan, A.Y.Y., Corey, J., Priebe, N.J., 2013. Emergence of Orientation Selectivity in the Mammalian Visual Pathway. J. Neurosci. 33, 10616. doi:10.1523/JNEUROSCI.0404-13.2013

Seabrook, T.A., Burbridge, T.J., Crair, M.C., Huberman, A.D., 2017. Architecture, Function, and Assembly of the Mouse Visual System. Annu. Rev. Neurosci. 40, 499–538. doi:10.1146/annurev-neuro-071714-033842

Sedigh-Sarvestani, M., Vigeland, L., Fernandez-Lamo, I., Taylor, M.M., Palmer, L.A., Contreras, D., 2017. Intracellular, In Vivo, Dynamics of Thalamocortical Synapses in Visual Cortex. J. Neurosci. 37, 5250. doi:10.1523/JNEUROSCI.3370-16.2017

Self, M.W., Lorteije, J.A.M., Vangeneugden, J., van Beest, E.H., Grigore, M.E., Levelt, C.N., Heimel, J.A., Roelfsema, P.R., 2014. Orientation-Tuned Surround Suppression in Mouse Visual Cortex. J. Neurosci. 34, 9290. doi:10.1523/JNEUROSCI.5051-13.2014

Sengpiel, F., Blakemore, C., 1996. The neural basis of suppression and amblyopia in strabismus. Eye 10, 250–258.

Sharpee, T.O., Sugihara, H., Kurgansky, A.V., Rebrik, S.P., Stryker, M.P., Miller, K.D., 2006. Adaptive filtering enhances information transmission in visual cortex. Nature 439, 936–942. doi:10.1038/nature04519

Sherman, S.M., Guillery, R.W., 1996. Functional organization of thalamocortical relays. J. Neurophysiol. 76, 1367.

Shou, T., Leventhal, A.G., Thompson, K.G., Zhou, Y., 1995. Direction biases of X and Y type retinal ganglion cells in the cat. J. Neurophysiol. 73, 1414.

Sigman, M., Cecchi, G.A., Gilbert, C.D., Magnasco, M.O., 2001. On a common circle: Natural scenes and Gestalt rules. Proc. Natl. Acad. Sci. U. S. A. 98, 1935–1940.

Silberberg, G., Markram, H., 2007. Disynaptic Inhibition between Neocortical Pyramidal Cells Mediated by Martinotti Cells. Neuron 53, 735–746. doi:10.1016/j.neuron.2007.02.012

Sillito, A.M., Cudeiro, J., Jones, H.E., 2006. Always returning: feedback and sensory processing in visual cortex and thalamus. Neural Substrates Cogn. 29, 307–316. doi:10.1016/j.tins.2006.05.001

Sillito, A.M., Jones, H.E., 2002. Corticothalamic interactions in the transfer of visual information. Philos. Trans. R. Soc. Lond. B. Biol. Sci. 357, 1739. doi:10.1098/rstb.2002.1170

Sincich, L.C., Adams, D.L., Economides, J.R., Horton, J.C., 2007. Transmission of Spike Trains at the Retinogeniculate Synapse. J. Neurosci. 27, 2683. doi:10.1523/JNEUROSCI.5077-06.2007

Sincich, L.C., Blasdel, G.G., 2001. Oriented Axon Projections in Primary Visual Cortex of the Monkey. J. Neurosci. 21, 4416.

Sjöström, P.J., Häusser, M., 2006. A Cooperative Switch Determines the Sign of Synaptic Plasticity in Distal Dendrites of Neocortical Pyramidal Neurons. Neuron 51, 227–238. doi:10.1016/j.neuron.2006.06.017

Sjöström, P.J., Turrigiano, G.G., Nelson, S.B., 2003. Neocortical LTD via Coincident Activation of Presynaptic NMDA and Cannabinoid Receptors. Neuron 39, 641–654. doi:10.1016/S0896-6273(03)00476-8

Sjöström, P.J., Turrigiano, G.G., Nelson, S.B., 2001. Rate, Timing, and Cooperativity Jointly Determine Cortical Synaptic Plasticity. Neuron 32, 1149–1164. doi:10.1016/S0896-6273(01)00542-6

Smith, S.L., Smith, I.T., Branco, T., Häusser, M., 2013. Dendritic spikes enhance stimulus selectivity in cortical neurons in vivo. Nature 503, 115–120. doi:10.1038/nature12600

Spruston, N., 2008. Pyramidal neurons: dendritic structure and synaptic integration. Nat Rev Neurosci 9, 206–221. doi:10.1038/nrn2286

Stepanyants, A., Martinez, L.M., Ferecskó, A.S., Kisvárday, Z.F., 2009. The fractions of short- and long-range connections in the visual cortex. Proc. Natl. Acad. Sci. U. S. A. 106, 3555–3560. doi:10.1073/pnas.0810390106

Stuart, G., Spruston, N., Sakmann, B., Häusser, M., 1997. Action potential initiation and backpropagation in neurons of the mammalian CNS. Trends Neurosci. 20, 125–131. doi:10.1016/S0166-2236(96)10075-8

Stuart, G.J., Sakmann, B., 1994. Active propagation of somatic action potentials into neocortical pyramidal cell dendrites. Nature 367, 69–72. doi:10.1038/367069a0

Stuart, G.J., Spruston, N., 2015. Dendritic integration: 60 years of progress 18, 1713.

Sun, W., Deng, Q., Levick, W.R., He, S., 2006. ON direction-selective ganglion cells in the mouse retina. J. Physiol. 576, 197–202. doi:10.1113/jphysiol.2006.115857

Suresh, V., Çiftçioğlu, U.M., Wang, X., Lala, B.M., Ding, K.R., Smith, W.A., Sommer, F.T., Hirsch, J.A., 2016. Synaptic Contributions to Receptive Field Structure and Response Properties in the Rodent Lateral Geniculate Nucleus of the Thalamus. J. Neurosci. 36, 10949. doi:10.1523/JNEUROSCI.1045-16.2016

Svoboda, K., Denk, W., Kleinfeld, D., Tank, D.W., 1997. In vivo dendritic calcium dynamics in neocortical pyramidal neurons. Nature 385, 161–165. doi:10.1038/385161a0

Svoboda, K., Helmchen, F., Denk, W., Tank, D.W., 1999. Spread of dendritic excitation in layer 2/3 pyramidal neurons in rat barrel cortex in vivo 2, 65.

Swadlow, H.A., 2003. Fast-spike Interneurons and Feedforward Inhibition in Awake Sensory Neocortex. Cereb. Cortex 13, 25–32. doi:10.1093/cercor/13.1.25

Takahashi, N., Kitamura, K., Matsuo, N., Mayford, M., Kano, M., Matsuki, N., Ikegaya, Y., 2012. Locally Synchronized Synaptic Inputs. Science 335, 353. doi:10.1126/science.1210362

Thomson, A., Lamy, C., 2007. Functional maps of neocortical local circuitry. Front. Neurosci. 1, 2. doi:10.3389/neuro.01.1.1.002.2007

Tien, N.-W., Pearson, J.T., Heller, C.R., Demas, J., Kerschensteiner, D., 2015. Genetically Identified Suppressed-by-Contrast Retinal Ganglion Cells Reliably Signal Self-Generated Visual Stimuli. J. Neurosci. 35, 10815. doi:10.1523/JNEUROSCI.1521-15.2015

Ts'o, D., Gilbert, C., Wiesel, T., 1986. Relationships between horizontal interactions and functional architecture in cat striate cortex as revealed by cross-correlation analysis. J. Neurosci. 6, 1160.

Turrigiano, G., 2011. Too Many Cooks? Intrinsic and Synaptic Homeostatic Mechanisms in Cortical Circuit Refinement. Annu. Rev. Neurosci. 34, 89–103. doi:10.1146/annurev-neuro-060909-153238

Turrigiano, G.G., Nelson, S.B., 2004. Homeostatic plasticity in the developing nervous system. Nat Rev Neurosci 5, 97–107. doi:10.1038/nrn1327

Usrey, W.M., Reppas, J.B., Reid, R.C., 1999. Specificity and Strength of Retinogeniculate Connections. J. Neurophysiol. 82, 3527.

Van den Bergh, G., Zhang, B., Arckens, L., Chino, Y.M., 2010. Receptive-field properties of V1 and V2 neurons in mice and macaque monkeys. J. Comp. Neurol. 518, 2051–2070. doi:10.1002/cne.22321

Van Hooser, S.D., Heimel, J.A.F., Chung, S., Nelson, S.B., Toth, L.J., 2005. Orientation Selectivity without Orientation Maps in Visual Cortex of a Highly Visual Mammal. J. Neurosci. 25, 19. doi:10.1523/JNEUROSCI.4042-04.2005

Vaney, D.I., Taylor, W.R., 2002. Direction selectivity in the retina. Curr. Opin. Neurobiol. 12, 405–410. doi:10.1016/S0959-4388(02)00337-9

Vogelstein, J.T., Packer, A.M., Machado, T.A., Sippy, T., Babadi, B., Yuste, R., Paninski, L., 2010. Fast nonnegative deconvolution for spike train inference from population calcium imaging. J. Neurophysiol. 104, 3691–3704.

Wang, Q., Burkhalter, A., 2007. Area map of mouse visual cortex. J. Comp. Neurol. 502, 339–357. doi:10.1002/cne.21286

Waters, J., Larkum, M., Sakmann, B., Helmchen, F., 2003. Supralinear Ca^{2+} Influx into Dendritic Tufts of Layer 2/3 Neocortical Pyramidal Neurons In Vitro and In Vivo. J. Neurosci. 23, 8558.

Weber, J.P., Andrásfalvy, B.K., Polito, M., Magó, Á., Ujfalussy, B.B., Makara, J.K., 2016. Location-dependent synaptic plasticity rules by dendritic spine cooperativity 7, 11380.

Weng, S., Sun, W., He, S., 2005. Identification of ON–OFF direction-selective ganglion cells in the mouse retina. J. Physiol. 562, 915–923. doi:10.1113/jphysiol.2004.076695

Werblin, F.S., Dowling, J.E., 1969. Organization of the retina of the mudpuppy, Necturus maculosus. II. Intracellular recording. J. Neurophysiol. 32, 339.

Wertz, A., Trenholm, S., Yonehara, K., Hillier, D., Raics, Z., Leinweber, M., Szalay, G., Ghanem, A., Keller, G., Rózsa, B., Conzelmann, K.-K., Roska, B., 2015a. Single-cell–initiated monosynaptic tracing reveals layer-specific cortical network modules. Science 349, 70. doi:10.1126/science.aab1687

Wertz, A., Trenholm, S., Yonehara, K., Hillier, D., Raics, Z., Leinweber, M., Szalay, G., Ghanem, A., Keller, G., Rózsa, B., Conzelmann, K.-K., Roska, B., 2015b. PRESYNAPTIC NETWORKS. Single-cell-initiated monosynaptic tracing reveals layer-specific cortical network modules. Science 349, 70–74. doi:10.1126/science.aab1687

Williams, S.R., Stuarty, G.J., 1999. Mechanisms and consequences of action potential burst firing in rat neocortical pyramidal neurons. J. Physiol. 521, 467–482. doi:10.1111/j.1469-7793.1999.00467.x

Wilson, D.E., Whitney, D.E., Scholl, B., Fitzpatrick, D., 2016. Orientation selectivity and the functional clustering of synaptic inputs in primary visual cortex. Nat. Neurosci. 19, 1003–1009. doi:10.1038/nn.4323

Wilson, H.R., Wilkinson, F., 2002. Symmetry perception: a novel approach for biological shapes. Vision Res. 42, 589–597. doi:10.1016/S0042-6989(01)00299-1

Wilson, N.R., Runyan, C.A., Wang, F.L., Sur, M., 2012. Division and subtraction by distinct cortical inhibitory networks in vivo. Nature 488, 343–348. doi:10.1038/nature11347

Xu, N., Harnett, M.T., Williams, S.R., Huber, D., O/'Connor, D.H., Svoboda, K., Magee, J.C., 2012. Nonlinear dendritic integration of sensory and motor input during an active sensing task. Nature 492, 247–251. doi:10.1038/nature11601

Xu, X., Callaway, E.M., 2009. Laminar Specificity of Functional Input to Distinct Types of Inhibitory Cortical Neurons. J. Neurosci. 29, 70. doi:10.1523/JNEUROSCI.4104-08.2009

XU, X., ICHIDA, J., SHOSTAK, Y., BONDS, A.B., CASAGRANDE, V.A., 2002. Are primate lateral geniculate nucleus (LGN) cells really sensitive to orientation or direction? Vis. Neurosci. 19, 97–108. doi:10.1017/S0952523802191097

Xue, M., Atallah, B.V., Scanziani, M., 2014. Equalizing excitation-inhibition ratios across visual cortical neurons. Nature 511, 596–600.

Yang, S.-N., Tang, Y.-G., Zucker, R.S., 1999. Selective Induction of LTP and LTD by Postsynaptic $[Ca^{2+}]_i$ Elevation. J. Neurophysiol. 81, 781.

Yarfitz, S., Hurley, J.B., 1994. Transduction mechanisms of vertebrate and invertebrate photoreceptors. J. Biol. Chem. 269, 14329–14332.

Yavorska, I., Wehr, M., 2016. Somatostatin-Expressing Inhibitory Interneurons in Cortical Circuits. Front. Neural Circuits 10, 76. doi:10.3389/fncir.2016.00076

Yeh, C.-I., Xing, D., Williams, P.E., Shapley, R.M., 2009. Stimulus ensemble and cortical layer determine V1 spatial receptive fields. Proc. Natl. Acad. Sci. U. S. A. 106, 14652–14657. doi:10.1073/pnas.0907406106

Yen, S.-C., Finkel, L.H., 1998. Extraction of perceptually salient contours by striate cortical networks. Vision Res. 38, 719–741. doi:10.1016/S0042-6989(97)00197-1

Yoshimura, Y., Callaway, E.M., 2005. Fine-scale specificity of cortical networks depends on inhibitory cell type and connectivity 8, 1552.

Yoshimura, Y., Dantzker, J.L.M., Callaway, E.M., 2005. Excitatory cortical neurons form fine-scale functional networks. Nature 433, 868–873. doi:10.1038/nature03252

Yu, Y.-C., He, S., Chen, S., Fu, Y., Brown, K.N., Yao, X.-H., Ma, J., Gao, K.P., Sosinsky, G.E., Huang, K., Shi, S.-H., 2012. Preferential electrical coupling regulates neocortical lineage-dependent microcircuit assembly. Nature 486, 113–117. doi:10.1038/nature10958

Yuste, R., Denk, W., 1995. Dendritic spines as basic functional units of neuronal integration. Nature 375, 682–684. doi:10.1038/375682a0

Yuste, R., Majewska, A., Holthoff, K., 2000. From form to function: calcium compartmentalization in dendritic spines 3, 653.

Zhao, X., Chen, H., Liu, X., Cang, J., 2013a. Orientation-selective Responses in the Mouse Lateral Geniculate Nucleus. J. Neurosci. 33, 12751. doi:10.1523/JNEUROSCI.0095-13.2013

Zhao, X., Liu, M., Cang, J., 2013b. Sublinear binocular integration preserves orientation selectivity in mouse visual cortex 4, 2088.

IOANA TEODORA GASLER i.gasler@unibas.ch +41788097797

PERSONAL INFORMATION

Date of Birth: Aug 17th 1989 Nationality: Romanian Gender: Female

EDUCATION

Sep 2013 – Nov 2017 PhD in Neurobiology, Biozentrum, University of Basel

Oct 2011 - Jun 2013 MSc in Neurobiology, Faculty of Biology, University of Bucharest
Dissertation grade: 10/10
Average grade for academic years: 9.93/10

Oct 2008 - Jun 2011 Bachelor in Biochemistry, Faculty of Biology, University of Bucharest
Thesis grade: 10/10
Average grade for academic years: 8.73/10

ACADEMIC WORK

Nov 2017 – present Post doctoral researcher with Prof. Dr. Sonja Hofer at Biozentrum, University of Basel, Switzerland

Sep 2013 – Nov 2017 PhD project with Prof. Dr. Sonja Hofer entitled "Synaptic representation of visual space in primary visual cortex" at Bioyentrum, University of Basel, Switzerland (Two-photon in vivo calcium imaging)

Sep 2011- Jun 2013 Research project with Prof. Dr. Alexandru Babes at University of Bucharest entitled: "Cellular and molecular mechanisms of diabetic neuropathy: immune system and glycation agents involvement" (Calcium imaging and whole-cell patch clamp on transiently transfected Hek 293 cells and primary sensory neurons, RT-PCR, viability assays).

Sep 2012- Oct 2012 Dissertation thesis project with Prof.Dr. Eric Lingueglia at Institut de Pharmacologie Moléculaire et Cellulaire (Sophia Antipolis, France) entitled "Distribution of ASIC ion channels in the murine nervous system". (Primer design, RT-PCR)

Jul 2012 Poster: "Prolonged exposure to methylglyoxal leads to increased expression of ion channels involved in pain- and temperature-sensing" presented at the 8th FENS Forum of Neuroscience, Barcelona, Spain.

Oct 2010- Jun 2011 Bachelor's thesis project with Prof. Dr. Alexandru Babes at University of Bucharest, Romania entitled: "Effects of chemotherapeutic agents on rat sensory neurons". (Calcium imaging on primary cultures of DRG neurons)

Feb - Oct 2010 Lab training in the Laboratory of Neurophysiology (group leader Prof. Dr. Alexandru Babes) at University of Bucharest, Romania. Project entitled: "Effect of Ruthenium Red on TRPM8 activation" (Calcium imaging on transiently transfected Hek 293 cells).

PUBLICATIONS

Iacaruso M.F, Gasler I.T, Hofer S.B. "Synaptic representation of visual space in primary visual cortex", Nature, 2017

Ciobanu A.C, Selescu T., Gasler I., Soltuzu L., Babes A. "Glycolytic metabolite methylglyoxal inhibits cold and menthol activation of the transient receptor potential melastatin type 8 channel", J Neurosci Res., 2016

TRAINING

26 – 28 July 2016 MATLAB Programing Techniques course by Mathworks, Cambridge UK

1 – 17 June 2013 FENS Transylvanian Experimental Neuroscience Summer School (TENSS), Pike Lake, Romania.During this hands-on intensive school I was introduced to many theoretical and practical aspects of microscopy, imaging, electrophysiology (especially in vivo recordings), animal handling and behaviour assays, as well as

programming (in LabView and MATLAB) for recordings and data analysis.

26 Nov – 1 Dec 2012 Experience exchange, Biomedical Research Foundation Academy of Athens, Athens, Greece. On this short stay I visited Dr. Epaminondas Doxakis's lab, whose research focus are K channels and miRNAs.

2 Sep – 28 Oct 2012 NENS Training Stay scholarship, Institut de Pharmacologie Moleculaire et Cellulaire, Sophia Antipolis, France. While in Dr. Eric Lingueglia's "Douleur et canaux ioniques" lab, I was trained in real-time PCR, with an emphasis on the primer design and testing phase preceding PCR experiments.

SKILLS

Cell cultures	Stable cell lines cultures (Hek 293, CHO) DRG neurons primary cultures
Molecular	MOLECULAR BIOLOGY Cell transfections DNA amplification Real Time RT-PCR Cloning IMAGING Wide field non-ratiometric calcium imaging Two photon in vivo calcium imaging Intrinsic imaging ELECTROPHYSIOLOGY Basic knowledge of whole-cell patch clamp recordings HISTOLOLOGY Immunostaining of brain slices
Animal	Surgeries, animal handling, training, in vivo recordings, perfusions. Swiss licence for animal experimentation.
Computing	OFFICE AND STATISTICS SOFTWARE - Advanced knowledge of MS Office and OriginPro PROGRAMMING - MatLab, basic LabView experience
Languages	Fluent English; Advanced French; Intermediate German; Basic Spanish, Italian, Dutch

INTERESTS

Travel, Hiking, Climbing, Sports, Reading, Languages.